Spatiotemporal Correlation Analysis of Jet Noise from a High-Performance Military Aircraft

Blaine M. Harker [1], Tracianne B. Neilsen [2], Kent L. Gee [3]
Brigham Young University, Provo, UT, 84602

Alan T. Wall [4]
Air Force Research Laboratory, Wright-Patterson Air Force Base, OH, 45433

and

Michael M. James [5]
Blue Ridge Research and Consulting, LLC, Asheville, NC, 28801

Correlation analyses of pressure measurements on a ground-based array of microphones of noise from a tethered F-22A provide insights into the sound field variation with position and engine conditions which are fundamental in the continued development of more complete jet noise models. Time-scaled, single-point (auto)correlation functions confirm that to the side of the nozzle exit, the temporal correlation envelope decays very rapidly, whereas the envelope decays more slowly in the maximum radiation region and farther downstream. Two-point space-time (cross) correlation functions reveal the variation in phase speed across the array and yield an estimate of the mean source region at each engine condition. In addition, the cross-correlation analysis confirms that noise from a single engine operating at intermediate power is more similar to that from heated, laboratory-scale jets, whereas additional features seen at military power and afterburner are unique. While one of these extra cross-correlation features may be related to plume-impingement of the concrete run-up pad, the other likely is related to the dual directivity lobe observed in the far field of military aircraft. Among the features of jet noise illuminated by a complementary coherence analysis are estimates of spatial coherence lengths as a function of frequency and location. The field coherence lengths are utilized in analyzing the coherence lengths of equivalent source distributions obtained from applying DAMAS-C to the ground-based array data. The cumulative results of these investigations provide a deeper understanding of jet noise source features and provide a full-scale military jet noise benchmark that should be considered when evaluating laboratory-scale jet studies and computational simulations of jet noise.

Nomenclature

A_{ab}	=	Envelope function between measurements $a(t)$ and $b(t)$
f	=	Frequency
$G_{ab}(f)$	=	Cross-spectral element between signals $a(t)$ and $b(t)$
$L_{\gamma^2}(x,f)$	=	Coherence length
R_{ab}	=	Correlation function between measurements $a(t)$ and $b(t)$
z	=	Downstream distance
γ^2	=	Coherence
η	=	Nondimensional time scale
τ	=	Time delay

[1] Graduate Student, Dept. of Physics and Astronomy, N283 ESC, AIAA Student Member.

[2] Part-Time Assistant Professor, Dept. of Physics and Astronomy, N283 ESC, AIAA Member.

[3] Associate Professor, Dept. of Physics and Astronomy, N283 ESC, AIAA Senior Member.

[4] Postdoctoral Research Fellow, Battlespace Acoustics Branch, AFRL 711 HPW/RHCB.

[5] Senior Principal Engineer, 29 N Market St, Suite 700, AIAA Member.

American Institute of Aeronautics and Astronautics

I. Introduction

Correlation analyses of near-field acoustical data from supersonic tactical aircraft engines provide key insights into the noise field variation as a function of location and engine power. While not unique, the jet noise source characteristics are imprinted on the radiated sound field,[1] thus the spatiotemporal characteristics found in the pressure field can provide a benchmark to help determine the applicability of laboratory-scale experiments, numerical simulations, and source models—e.g., beamforming and wavepackets methods to the modeling of full-scale, heated, supersonic jet noise—more completely than spectral analysis alone. Within the jet noise community, the two-point, space-time pressure correlation functions in the near field[2-4] and the shape of single-point pressure autocorrelation functions have been used to interpret the nature of the radiation as a function of downstream location or far-field angle.[1, 5] They have also been used to provide spatiotemporal length scales, either broadband[1] or band-limited,[6] which are useful in validating and improving jet noise models.[7-10] The unique correlation results presented in this paper for full-scale tactical engine noise significantly expand the growing number of laboratory and computational jet studies that use auto (single-point) and cross (two-point) correlation functions of the acoustic field to obtain not only valuable information on the spatial structure of the noise field, but also insights into the noise sources represented by the turbulent jet plume.

The results of the full-scale analysis of pressure waveforms acquired at a ground-based microphone array provide insight and a basis to compare the noise from an installed F-22A engine against other studies. Early work by Clarkson,[11] Fuchs,[12, 13] and Fisher et al.[14] as well as more recent work by Tam et al.[1] have suggested the autocorrelation function has significant negative loops when large-scale structure noise dominated the spectrum. This was verified by Harker et al.,[5] who calculated autocorrelation functions defined by Tam's large and fine-scale similarity spectra[15, 16] and showed that the autocorrelation function of the large-scale similarity spectrum contains significant negative loops. Viswanathan et al.[4] used an extensive conical array of microphones to calculate near-field correlation measurements of a laboratory-scale, heated supersonic jet. They determined that a large coherent region existed, located in the near field at least two potential core lengths downstream and beyond the maximum radiation region, as well as a single mechanism responsible for the generation and radiation of noise to the peak radiation sector. Kumar et al.[17] showed how the temporal width of the far-field correlation measurements broadened as a laboratory-scale jet was operated at under, ideally and over-expanded conditions. Liu et al.[18] calculated cross correlations as part of an analysis of numerical pressure fields resulting from simulations of perfectly expanded and underexpanded jets. They found that while the broadband shock-associated noise (BBSAN) could be identified in the cross correlation, the autocorrelation distribution gives a more precise end location of the BBSAN. In the downstream region, the mixing noise and the BBSAN distributions become similar except that the correlation values of the large-scale noise are larger than the BBSAN-containing distribution. However, they also caution that because a large correlation is not necessarily indicative of source characteristics, spatial trends have to be carefully examined.

Correlation measurements have also been prevalent in examining the connection between flow parameters and the acoustic field. Panda et al.[19, 20] conducted correlation measurements of the source region comparing far-field acoustic pressure measurements to density and jet velocity measurements within the source plume for subsonic and supersonic unheated jets at laboratory-scale. They found that correlation between density and velocity parameters was greatest in the downstream radiation direction, corresponding to large coherent structures. Furthermore, they found cross-correlation to be greatest when measured at the jet centerline. Papamoschou et al.[21] compared beamformed pressure measurements in the acoustic field to flow parameters in the mixing region using optical deflectometry measurements. They found significant correlation between far-field acoustic measurements and the flow parameters in the jet shear layer, particularly in the mixing region and outside of the hydrodynamic field. They also noted that the peak correlation coefficients were slightly downstream of their probe location in the flow field, highlighting the effects of refraction in beamforming models. Baars et al.[22] used the two-point space-time correlation functions to estimate the convective (phase) speeds of noise across a linear array of microphones located in the hydrodynamic near field of unheated and heated Mach 1.5 jets, finding that, between 11 – 20 jet nozzle diameters downstream, the convective speed decreases significantly with distance, corresponding to the decay of large-scale turbulent structures. They also measured coherence across the array and showed coherence lengths across the array which spanned multiple jet nozzle diameters depending on frequency. When comparing heated and unheated cases, they noted a decrease in coherence length.

In this paper, spatiotemporal correlation and coherence analyses of sound measured in the vicinity of a static F-22A Raptor are presented to provide an improved characterization of the noise radiation and to provide a benchmark case for comparing against modeling and laboratory-scale experiments. A brief introduction to correlation methods is followed by a short description of the experiment. Single-point and two-point correlation functions of the pressure

2

field, referred to as auto and cross correlations, respectively, from an array of ground-based microphones in the vicinity of an F-22 aircraft at intermediate, military and afterburner condition are presented to investigate the broadband features of the sound field. Some of the F-22 correlation features are not exhibited in previous laboratory-scale jet studies. To investigate these features further, a complementary study of the coherence of the noise at select frequencies is presented to provide additional insights. The final analysis presented in this paper seeks to relate the properties of the field coherence to estimates of the source coherence obtained from a variation of a beamforming algorithm called deconvolution and mapping of acoustic sources that account for potential source coherence, called DAMAS-C.[23, 24] Findings thus far yield a more complete picture of tactical jet noise characteristics and highlight features of noise from high-performance military aircraft that have not yet been replicated in laboratory-scale jets.

II. Correlation Methods

The correlation between two waveforms is defined as[25]

$$R_{ab}(\tau) = E[a(t)b(t + \tau)] \tag{1}$$

where the expectation value, $E[\cdot]$, of a signal $a(t)$ with a signal $b(t)$ delayed by time τ. For zero-mean signals, the correlation function is also the covariance function. A single-point correlation function, also known as the autocorrelation, $R_{aa}(\tau)$ is the inverse Fourier transform of the autospectrum. This property is what allowed Harker *et al.* to develop similarity autocorrelation functions from Tam's fine and large-scale similarity spectra.[5] Similarly, a two-points correlation function, the cross correlation, $R_{ab}(\tau)$, and the cross spectrum form a Fourier transform pair. Although the correlation and the spectrum technically contain the same information, it is sometimes beneficial to use one of them to more easily examine different sound field trends. For example, periodicity in the waveform are easily identified using the correlation function, and measurements of spatiotemporal length scales and phase speeds may be obtained. In this paper, all correlation functions are normalized by the maximum correlation value, i.e. as correlation coefficients, such that $|R_{ab}(\tau)|^2 \le R_{aa}(0)R_{bb}(0)$.

To facilitate the comparison of the temporal decay rates of $R_{ab}(\tau)$, the envelope function of the correlation coefficient is defined as[25]

$$A_{ab}(\tau) = [R_{ab}^2(\tau) + \tilde{R}_{ab}^2(\tau)]^{1/2}, \tag{2}$$

where $\tilde{R}_{ab}(\tau)$ is the Hilbert transform of the correlation coefficient. The envelope function is useful to more consistently quantify differences in the temporal decay rate of $R_{ab}(\tau)$ for various locations around a jet or for jets of different scales and conditions. Additionally, since $A_{aa}(\tau)$ is a positive function, it can be plotted on a logarithmic scale to more clearly observe low-amplitude features not visible in $R_{ab}(\tau)$. Finally, a spatial measure of the correlation can be accomplished by defining a length scale from the maximum cross correlation coefficients as the greatest distance from a given reference location with signal $a(t)$ over which $\max[R_{ab}(\tau)] > 0.5$.

The frequency-domain coherence function is related to the cross correlation as well, and is defined as

$$\gamma_{ab}^2(f) = \frac{|G_{ab}(f)|^2}{G_{aa}(f)G_{bb}(f)}. \tag{3}$$

The normalization by the autospectra results in a maximum coherence of unity. Note that coherence is calculated on a frequency-by-frequency basis, whereas correlation is defined for the entire waveform spectrum. Building on work from Wall *et al.*,[6] a coherence length, $L_{\gamma^2}(z_1, f)$, may be defined as the distance at which the coherence, $\gamma_{ab}^2(f)$, of a reference signal at z_1 drops to 0.5 when with compared to adjacent measurements z_i. Here, we distinguish between coherence lengths in the upstream and downstream measurement directions (parallel to the jet centerline axis) by $L_{\gamma^2}^-(z, f)$ and $L_{\gamma^2}^+(z, f)$, respectively.

Correlation studies have also been applied to understand properties of correlation at the source region. For example, beamforming measurements have been used in multiple contexts in attempts to reconstruct source properties from jet noise radiation,[26-29] Using phased arrays, pressure measurements are used to source reconstructions by defining a source distribution region in the vicinity of the jet plume. In this study, flow parameters and refraction effects are not incorporated to the beamforming model, hence an equivalent source region is obtained, which, nevertheless, provides a benchmark for future beamforming studies. Generally, beamforming analyses assume a distribution of incoherent simple sources. Because of the partially correlated sources found in jet noise, a study was

3

done by Harker *et al.*[10] using amplitude-weighted source distributions demonstrated the degree to which an incoherent-monopole assumption results in source reconstruction errors when correlated sources are present. However, Harker *et al.* also showed that methods based on the principles of cross-beamforming, which do not assume a specific source correlation, can accurately predict source levels and distributions when correlated sources are present. One such algorithm is an extension of the deconvolution and mapping of acoustical sources (DAMAS), known as DAMAS-C, which is favorable for jet noise studies because of its ability to reconstruct sources with varying degrees of correlation. A detailed description of the DAMAS-C algorithm can be found in Ref. [10]. Of importance here, however, is our finding that a beamformed source coherence can be obtained with DAMAS-C. While source level can usually be obtained as a function of space and frequency using traditional beamforming methods, DAMAS-C also determines a relationship in level and phase between two source locations. The algorithm is applied to each frequency component individually and we assume that the coherence, $\gamma^2_{z_1 z_2}$, relates a source located at a position z_1 along the jet centerline to another source at z_2 by their corresponding beamforming outputs:

$$\gamma^2_{z_1 z_2}(f) = \frac{\left|X_{z_1 z_2}(f)\right|^2}{X_{z_1 z_1}(f) X_{z_2 z_2}(f)}. \tag{4}$$

Here, $X_{z_1 z_2}(f)$ represents the DAMAS-C output due to the likelihood of sources at locations z_1 and z_2, along the jet centerline, generating the measured pressure field. $X_{z_1 z_1}(f)$ and $X_{z_2 z_2}(f)$ are the equivalent squared pressure source levels at z_1 and z_2 respectively. Because DAMAS-C outputs each of these values, the coherence, which relates the DAMAS-C output to the two measurement locations, can be obtained. The ascertaining of coherence from the DAMAS-C method is a direct consequence of the algorithm results and provides a unique contribution for its usage. The difficulty in the implementation of DAMAS-C is typically due to its high computational expense, which requires on the order of N^4 operations per scan point in a reconstruction plane. To address this, a one-dimensional source distribution along the jet centerline is chosen with a 0.3 m spacing between each scan point such that each frequency run was reduced from days of computation time to hours.

III. Experimental Setup

Noise measurements were made of a Pratt and Whitney model F119-PW-100 turbofan engine installed on Lockheed-Martin/Boeing F-22A Raptor (see top left plot in Fig. 1). The measurements, conducted July 2009 at Holloman Air Force base, were made jointly by the Air Force Research Laboratory, Blue Ridge Research and Consulting, LLC, and Brigham Young University. One of the engines on the tied-down aircraft was operated at four engine conditions (idle, intermediate (80%, Int), military (100%, Mil), and afterburner (AB)) while the other was held at idle. The tests were conducted on a concrete run-up pad (see bottom right photo of Fig. 1), which may be a source of low-level impingement noise. An array of 50 GRAS 6.35-mm and 3.18-mm microphones was placed on the ground 11.6 m from the centerline of the jet axis. As shown in the top left corner of Fig. 1, the ground array element spacing was 0.61 m, and the array spanned 30 m. Each measurement was taken for 30 seconds at either a 48 kHz or 96 kHz sampling rate, depending on the engine condition tested, and each resultant waveform was divided into time-waveform blocks of 2^15 samples each with 50% overlap. The top right results of Fig. 1 show the averaged overall sound pressure levels (OASPL) over the entire measurement set along with a band representing a standard deviation above and below the mean level. A Fourier transform was applied to each Hanning-windowed block, and cross-spectral calculations were averaged over the blocks to obtain cross-spectral density elements. For this experiment, the auto-spectral values of the cross-spectral matrix were included when the beamforming output was calculated, as it was found to improve resolution for regions with low beamforming response. A detailed description of the experiment is found in Ref. [30], and the spectral variation of the measured sound as a function of angle is shown in Ref. [31].
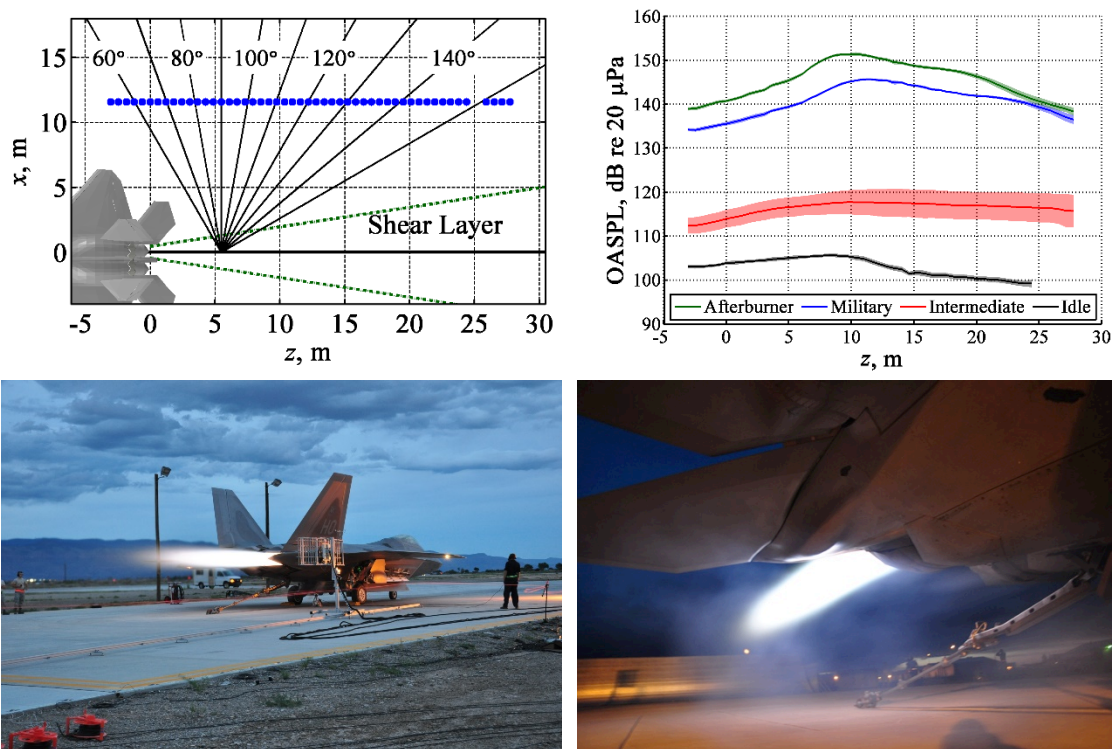
American Institute of Aeronautics and Astronautics

Figure 1 Experimental Setup. *(Top left) Schematic of noise measurements on an F-22A Raptor. (Top right) Overall sound pressure levels across the 50-microphone ground array located 11.6 m to the sideline of the jet centerline. (Bottom) Photographs from the F-22A test. The ground array is located just inside the edge of the pavement on the bottom left photo. In the bottom right photo, the jet is shown at afterburner positioned over the concrete run-up pad.*

The one-third octave (OTO) band spectra of the F-22 measurement at three engine operation conditions are shown as a function of position, z, along the ground-based array in Fig. 2. An extensive analysis of the spectral measurements and individual contributions due to large and fine-scale turbulent structures has been presented by Neilsen *et al.*[31] Of import here are the variations in peak frequency at each engine condition as a function of z. Radiation to the sideline, defined as 4 m < z < 6 m, and upstream (z < 4 m) exhibits spectra which are broad in nature and generally contain a higher peak frequency (approx. 800 – 1200 Hz). Farther downstream, the peak frequency drops to between 100-200 Hz and the spectral shapes become more peaked in nature. Across most of the array, the spectral shape has a single peak frequency with a continual decline above and below it, as has been observed for laboratory-scale jets.[4, 29] However, there also exist regions where two competing frequencies combine to produce a double-peaked spectral shape. Such a transition region exists at both Mil and AB in approximately the 12 m < z < 15 m range where two dominant frequencies exist in the spectra. This was also observed by Neilsen *et al.*,[32] who showed that the double-peak in the spectra was not accounted for by spectral shapes given by Tam *et al.*[15, 16] and also not present in existing laboratory-scale measurements. Note that a similar double peak has been noted in F-35 AA-1 data by Neilsen *et al.*[33] and in far-field F-22A data by Gee *et al.*[34] so this feature can be described as characteristic of current-generation tactical aircraft.

5

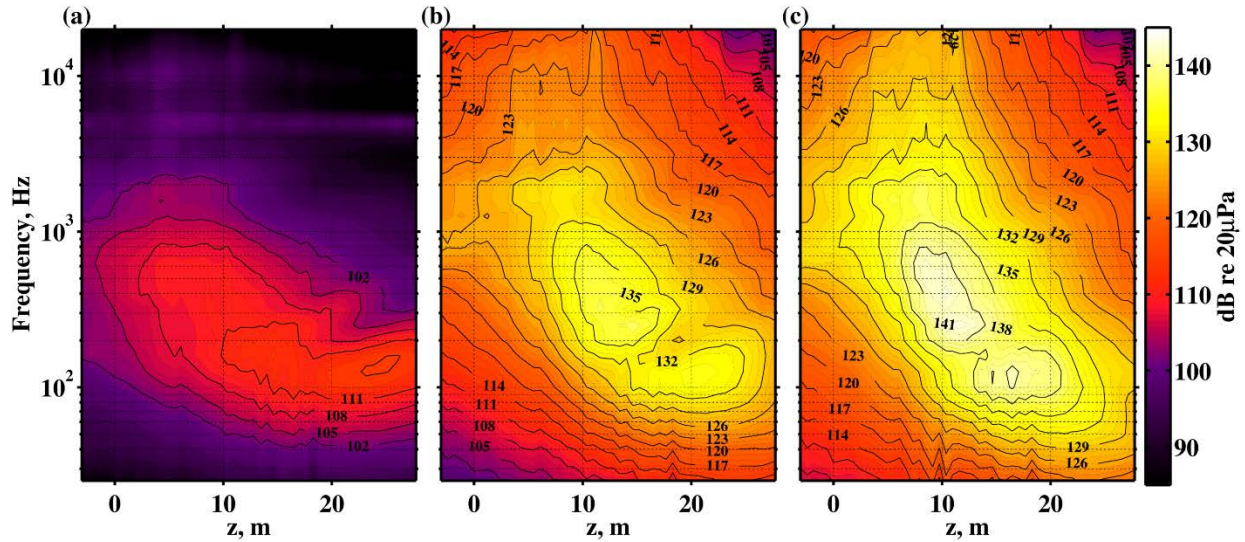American Institute of Aeronautics and Astronautics

Figure 2. One-third octave band sound pressure levels. *One-third octave band spectra for each of the 50 ground-based microphone located 11.6 m to the sideline of an F-22 when one engine was operated at (a) intermediate, (b) military, and (c) afterburner engine power.*

IV.   Analysis and Discussion

We first present a broadband analysis of full-scale jet correlation measurements using single-point and two-point correlation techniques in Sec. A to obtain temporal and spatial waveform characteristics. This provides a general overview of the spatial variation in the waveform features and an estimate of the phase speed, mean source region, and spatial correlation lengths of the sound field. Because some features within jet noise are frequency-dependent, the correlation investigation is augmented by a coherence analysis in Sec. B, which provides spatial scales of frequency-separated elements. The resulting field coherence maps provide estimates of the coherence lengths as described in Sec. II. The connection between the field coherence and the self-coherence of the source is also of interest. Hence, in Sec. C, source coherence measurements are obtained using the DAMAS-C beamforming algorithm and compared with the corresponding field coherence measurements.

A. Broadband Analysis

Because turbulent mixing noise is comprised of broadband, partially coherent structures that give rise to Mach wave radiation, the sound radiation properties over a broad frequency range are of interest. Unlike spectral or other narrowband analyses, the broadband nature of the jet noise is best studied using time-domain correlation analyses.[35] In this section, the single-point correlation functions are useful to understand the temporal scales over which the waveform is correlated, and measurements taken about the jet show the evolution of these properties in space. In addition, two-point correlation functions provide a look at the spatiotemporal variation in the correlation length scales and elucidate the properties found in the source region.

1. Single-point correlation measurements

The autocorrelation measurements of the ground-based array pressure measurements of the F-22 are presented Fig. 3 for various locations along the ground-based array for Mil engine condition. Sideline characteristics are generally marked by narrow correlation lengths (relative to the downstream) and contains small negative cusps, as seen for $z = 6$ m. Far downstream, $z > 15$ m, the width of the central peak in the autocorrelation functions is much larger and a single set of negative loops is more pronounced. This is observed at the three farthest downstream measurements shown. Tam *et al.*[1] show similar autocorrelation measurements for a laboratory-scale measurement and note that the large negative loops corresponds to the onset of noise due to large-scale turbulent structures. Harker *et al.*[5] showed that autocorrelation measurements of the similarity spectra defined by Tam *et al.*[15, 16]—which correspond to the large and fine-scale turbulent structures—share strong commonalities with these autocorrelation measurements. In particular, the similarity spectra associated with fine-scale turbulence is relatively narrow in width (i.e. correlated

6

American Institute of Aeronautics and Astronautics

over a shorter timespan) and shows shallow negative cusps, while the large-scale spectra shape is broader with a slower temporal decay and includes large negative loops.

In addition, two distinct differences exist which were not seen in previous laboratory measurements. First, in the upstream direction ($z \leq 0$ m), negative loops appear which are much larger than would be expected from small-scale similarity structures. While not seen in the OTO similarity spectra in Fig. 2(b), this relates to a strong peaked feature in the spectral data and may be indicative of broadband shock-associated noise. Second, autocorrelation measurements at 12 m and 15 m show an additional set of large negative loops. While measurements that are dominated by screech tones contain additional sets of negative loops (e.g. see Ref. [17]), it is not the case here because screech tones typically occur farther upstream and significant negative loops beyond the second pair are not present. The microphones over which these secondary loop occur, about 10-15 m downstream of the nozzle exit, are in the Mach wave radiation region where two peak frequencies coalesce, as shown in Fig. 2(b).

While the width of the autocorrelation functions has been associated with various features in the jet noise, there is a strong dependence on the associated peak frequency at each measurement location. In Fig. 3, the right block contains the autocorrelation for the same microphones, but plotted as a function of scaled time: $\eta = \tau \cdot f_{\text{peak}}$, where $f_{\text{peak}}(z)$ is the peak frequency at a given spatial location along the measurement array. When scaled by peak frequency, the width of each function is more similar both in the upstream and downstream measurement locations, with the first set of negative loops occurring at approximately $\eta = \pm 0.5$. Thus, the negative loops relate to the strong anti-correlation that exists in the waveforms extending at least one half-cycle in time relative to the peak frequency. There are also strong similarities in the scaled autocorrelation at -3 m and measurements farther downstream such as 21 m, indicating a more narrowband spectrum. At the 0 m and 6 m locations, the scaled autocorrelation widths are also similar to those downstream, yet they lack the characteristic negative loops indicative of partially correlated noise. Furthermore, the turning points are much more abrupt, as also seen in the autocorrelation function defining Tam's fine-scale similarity spectrum.[5] In the double loop region, the first set of loops occurs at $\eta \sim \pm 0.5$, although the other occurs $\eta \sim \pm 1.3$. Hence, the width of the central peak of the autocorrelation as a function of τ is foremost a function of the peak frequency in the signal, whereas the presence of negative loops contains information about the degree to which the signal is correlated in time.
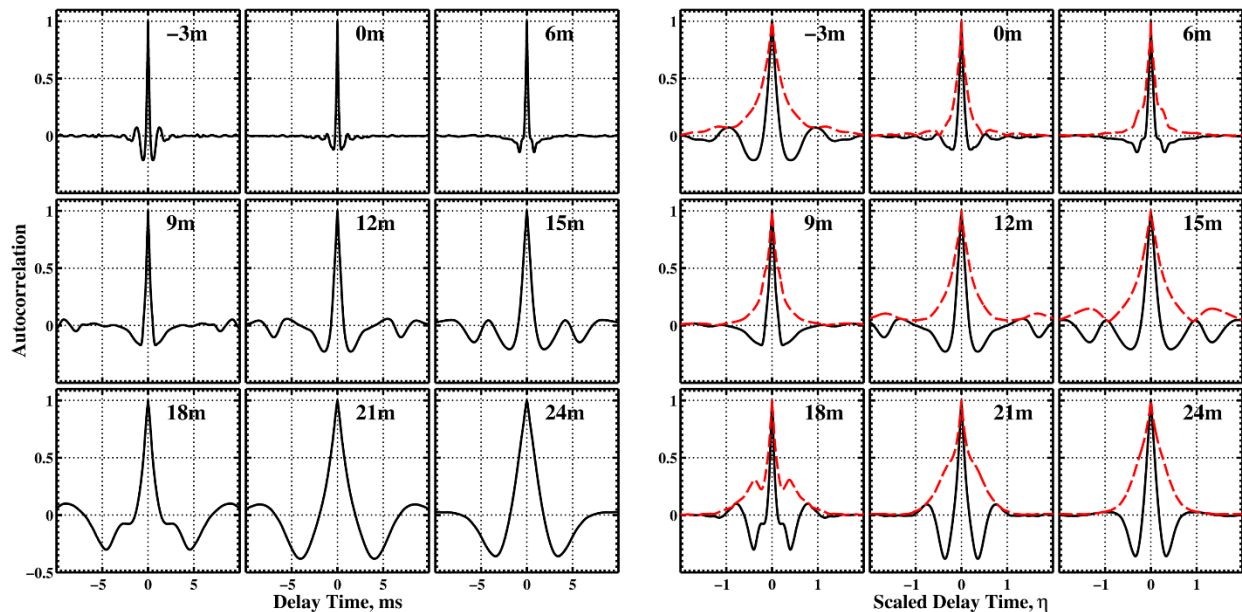

Figure 3. Autocorrelation functions at different ground-based microphones for the F-22A Raptor at military power. *The corresponding downstream distances are indicated on the individual frames. The time-scaled versions, $R_{xx}(\eta)$, are on the right, in which the spatial variation in the peak frequency has been removed, and autocorrelation envelopes, $A_{xx}(\eta)$, are overlaid on each as dashed lines.*

To better understand the physical significance of the negative loops, we consider samples of the waveforms at two array locations, shown in Fig. 4. The autocorrelation at each location is shown, with markers indicating key locations. At 15 m, the autocorrelation contains two negative loops spaced at approximately $\eta = \pm 0.5$ and ± 1.3. A sample of

7

the waveform is shown, which when calculating the autocorrelation produces unity by definition. Next, the waveform is overlaid by the same sample but with a delay time equal to $\eta = 0.5$. When the delay is applied, the waveform samples align in such a way that there is large anti-symmetry, creating the large negative loops seen in the autocorrelation. When the delay is applied in Fig. 4(d), there is also significant anti-symmetry, although to a slightly lesser degree. Note that the delay times here are not related by integer values, signifying that the two strong contributors are not harmonically related. At the 24 m measurement location, the waveform sample is overlaid by the same sample but with a delay time $\eta = 0.35$, which also produces strong anti-symmetry creating the large negative loop in the autocorrelation measurement. It is interesting to note that while the delay is approximately $\eta = 0.5$, it is not exactly related to the peak frequency at this location and may be due to an asymmetry in the levels below and above the peak frequency spectra. When the delay applied is $\eta = 1$ as seen in Fig. 4(h), there are no consistent patterns in the symmetries of the waveforms, resulting in a low autocorrelation value. Tam $et\ al.$[1] attributed this type of behavior in the waveform and corresponding autocorrelation measurement to the random impulse-like events in the jet noise radiation that is self-similar over the length of a single impulse and uncorrelated with other impulse-like features. Kearney-Fischer[36] also supports this theory with statistical investigations of the frequency of occurrence of intermittent events and shows that they do not influence one another. Indeed, there is evidence that these random events within the waveform share similarities such as a characteristic frequency, yet because the correlation is not significant beyond $\eta = 2$, these impulse-like events in the waveform are not consistent in temporal separation.
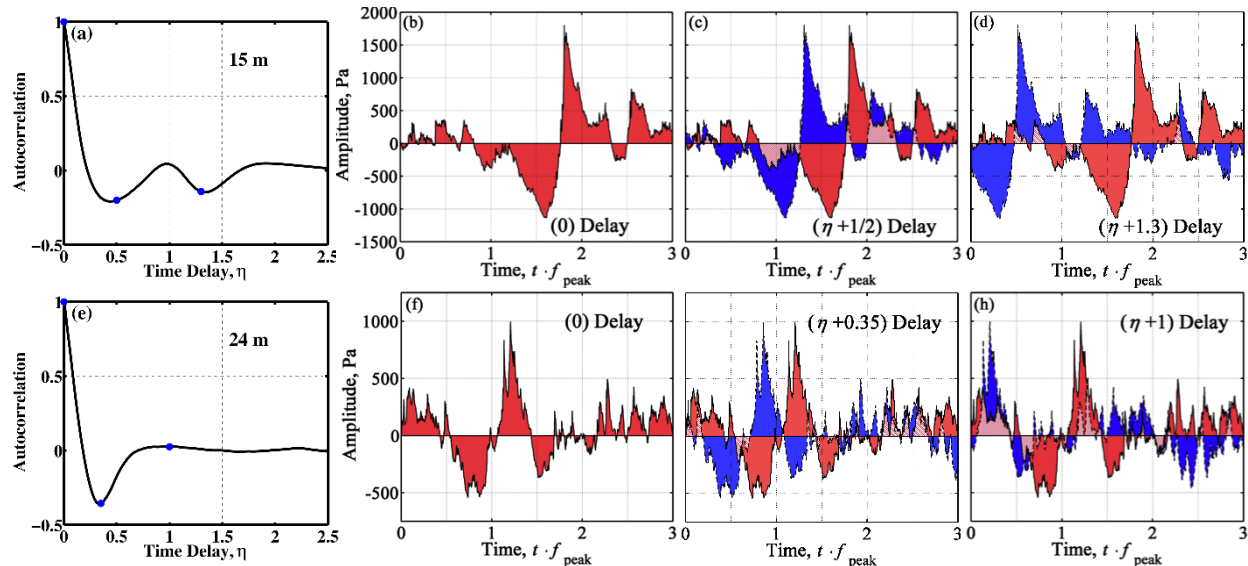

Figure 4. Shifting waveforms in time to calculate autocorrelation. *Waveform selection from ground-based array at (top) 15 m and (bottom) 24 m downstream.(a)/(e) Autocorrelation measurement with three locations marked. At 15 m, waveforms are overlaid with the same waveform at (b) $\eta = 0$ delay, (c) $\eta = 0.5$ delay (d) $\eta = 1.3$ delay. The same is done for the 24 m measurement with (f) $\eta = 0$ delay, (g) $\eta = 0.35$ delay (d) $\eta = 1$ delay. Waveforms are plotted in solid colors with a stripped pattern marking overlap between the two.*

The autocorrelation envelope, derived using Eq. (2), shows the magnitude of temporal correlation and provides the ability to measure the temporal decay (see Sec II).[5] It is shown overlaid on the scaled autocorrelation measurements in Fig. 3. The general trend of the envelope measurements is a smooth decay from the peak magnitude to a tapering off to zero. This is particularly seen in the downstream measurements with some variations. For example, at 12 m and 15 m there exist local minima in the envelopes at approximately $\eta \cong \pm 1$ followed by a secondary rise. As illustrated in the spectral data and waveform examples, the two competing peak frequencies destructively interfere when the time lag is approximately one cycle. At the sideline location, the envelope measurements decay more rapidly to zero, although the decay is not as smoothly defined as the downstream locations. At -3m and 0 m there are small secondary positive loops suggesting some small contribution from an additional feature.

A view of the spatial progression of the autocorrelation functions is useful to examine the variation with engine condition. Autocorrelation functions are shown in Fig. 5(a)-5(c) for the three engine conditions. The general observation across all engine conditions is the change in the width of the autocorrelation to be widest in the downstream direction. There also appear deep negative loops in the downstream direction, although the depth and onset location varies by engine condition. In the intermediate engine, the negative loops gradually develop between

American Institute of Aeronautics and Astronautics

$\tau = \pm(3 - 5)$ ms until they are fully visible for $z > 15$ m. In the Mil and AB engine cases, however, the onset of the negative loops occur as "winged" structures, developing at larger time delays, τ, until fully visible downstream. Similar laboratory-scale measurements have been shown which are similar to the intermediate engine case (e.g. see Ref. [18]), although the additional features previously mentioned in the Mil and AB cases have not been observed at the lab-scale. Liu *et al.*[18] observed that in autocorrelation measurements with and without shock content, additional ringing occurs for values τ beyond the initial negative loop. This similar effect is seen for the autocorrelation at Mil and AB for $z < 10$ m. In the Mil condition, the large negative loops seem to reach a minimum time delay approximately $\tau = \pm 3$ ms, before decaying beyond $z = 25$ m. In the afterburner case, the negative loops reach a minimum time delay of about ± 3 ms at $z = 18$ m before decaying and diverging to larger values of τ. These regions do not necessarily coincide with the maximum radiation regions, but rather with the lower frequency radiation. The secondary set of negative loops is also visible in the Mil and AB cases near $z = 13$ m and follows the expansion of the autocorrelation width until merging with the larger negative loop set farther downstream.
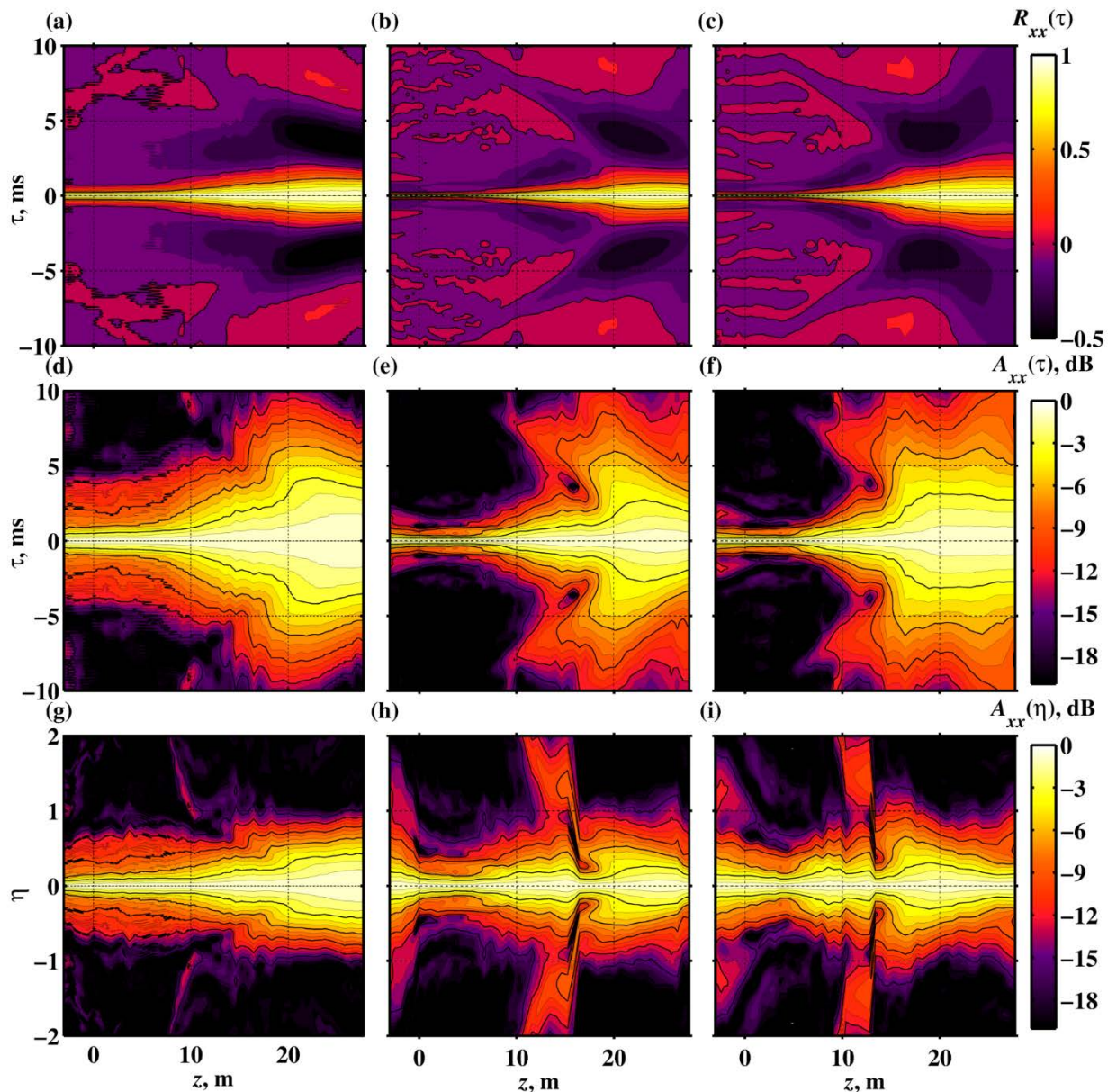

Figure 5. Autocorrelation function as a function of downstream distance. *(Top)* $R_{xx}(\tau)$ *at ground-based array for (a) Int, (b) Mil, and (c) AB. (Middle) The corresponding envelope functions, $A_{xx}(\tau)$ shown on a decibel scale for the*

9

American Institute of Aeronautics and Astronautics

three engine conditions in (d)-(f), and the time-scaled envelope functions. (Bottom) $A_{xx}(\eta)$ shown for the three conditions in (g)-(i).

Autocorrelation envelopes are shown (in decibels) in Fig. 5(d) – 5(f) for the three engine conditions. This allows for a comparison of the temporal decay of the autocorrelation over distance. In the intermediate engine case, the envelope width increases gradually with downstream distance until reaching a limiting value near $z = 20$ m before decreasing. In the Mil and AB cases, two features are particularly interesting. First, the envelope functions show a smooth decay in the downstream region except near $z = 15$ m where the two peak frequencies dominate. It is interesting to note that here there are locations at $\tau = \pm 4$ ms where the autocorrelation envelope drops below 20 dB, indicating a lack of correlation due to the two peak frequencies. Second, it is easy to identify the most correlated regions using these functions, such as the far upstream locations and in the downstream regions beyond the maximum radiation region. The time-scaled autocorrelation envelopes are shown in Fig. 5(g) – 5(i) to better understand what might be obscured by the strong variability of the peak frequency with distance. When scaled by peak frequency, the results for the different engine conditions are much more similar in width. However, even with the peak frequency-scaling, the envelope widths grow as a function of downstream distance such that the downstream measurements are generally larger than those at the sideline. Two exceptions to this, however, are found in the far upstream direction where BBSAN may be a factor, and in the far downstream direction beyond the Mach-wave radiation lobe.

2. Cross-correlation Analysis

Two-point, space-time correlation functions (hereafter referred to simply as cross correlation) provide added insight beyond the temporal scales from the autocorrelation functions as spatial length scales of the measurement help to better understand the spatial evolution of the source radiation. Because acoustic source features are imprinted on the two-point, space-time correlations,[2, 4, 20, 22] we apply this method here for measurements across the ground-based array near the F-22. The ensemble, averaged cross-correlation functions are calculated using the inverse Fourier transform of the cross spectrum,[25] and the spatial variation is examined for a number of reference microphones along the 50-microphone, ground-based array, depicted in Fig. 1. The widths of the cross-correlation functions relate to the temporal similarities in the waveforms between each array element to understand the nature of the sound received at a pair of microphones. [1, 8] As an extension of the autocorrelation functions, the width of a cross-correlation measurement, measured across the peak value, is related to the peak frequency of each waveform, but also to the spatial evolution of this content along the measurement array. Uncorrelated measurements produce narrow cross-correlation functions, whereas waveforms that are somewhat correlated yields wider cross-correlation functions. Additionally the time of arrival is imprinted on the cross correlograms such that the phase speed of the propagating wavefronts along the array can be estimated. This estimate is used to give rough approximations of the primary source region in the jet at the multiple engine conditions to ensure consistency with the results of more sophisticated source localization methods. Finally, the maximum cross correlation coefficients are compared to realize the variation in spatial length scales of the waveform correlation.

The two-point, space-time correlation measurements in the vicinity of the F-22 show the spatial variation in the noise and thus are intrinsically related to the partially correlated nature of the sound field. Normalized cross correlation functions for six reference microphones are displayed in Fig. 6, distributed along the 50-microphone ground array, when the F-22 engine was operated at military power, with the axial distance between each microphone spanning 0.6 m. Slightly upstream of the nozzle exit (top left) the maximum correlation between a measurement at -2 m and adjacent measurement locations is less than 0.5 and drops off rapidly with increasing distance. When the reference microphone is at 4 m downstream of the nozzle exit, the decay in the correlation peak is even more rapid and similar to what is expected for uncorrelated noise. For the reference at $z = 10$ m, the distance over which there is large correlation begins to expand and the timespan over which correlation is significant lengthens, which is likely related to the decrease in the peak frequency at this location. Asymmetry is also evident when comparing cross correlation measurements with upstream microphones to the downstream microphones, which is indicative of the directional Mach wave radiation. At $z = 15$ m, there is a dramatic change in the correlation functions to contain both a substantially larger spatial region of high peak correlation coefficients and larger temporal correlation. Both spatial and temporal scales grow, as does the prominence of the loops, as downstream distance increases. The variation in behavior with distance aligns with those discussed with respect to the autocorrelation and with previous spectral analyses.[32] Tam *et al.* [1] argued that the main difference in spatial variation of the cross-correlation was due to the length scales of turbulent structures which correspond to distinct temporal lengths in the waveform. Fine-scale structures create a field of random narrow pulses which are uncorrelated in space due to the small timespan of each pulse and the simultaneous measurement of multiple small-scale pulses. In contrast, large-scale structures emit

10

American Institute of Aeronautics and Astronautics

impulses with large timespans which create large bands of acoustic disturbances and thus a more correlated field. Here, the directional nature of the radiation in the downstream direction also contributes to a more correlated field.
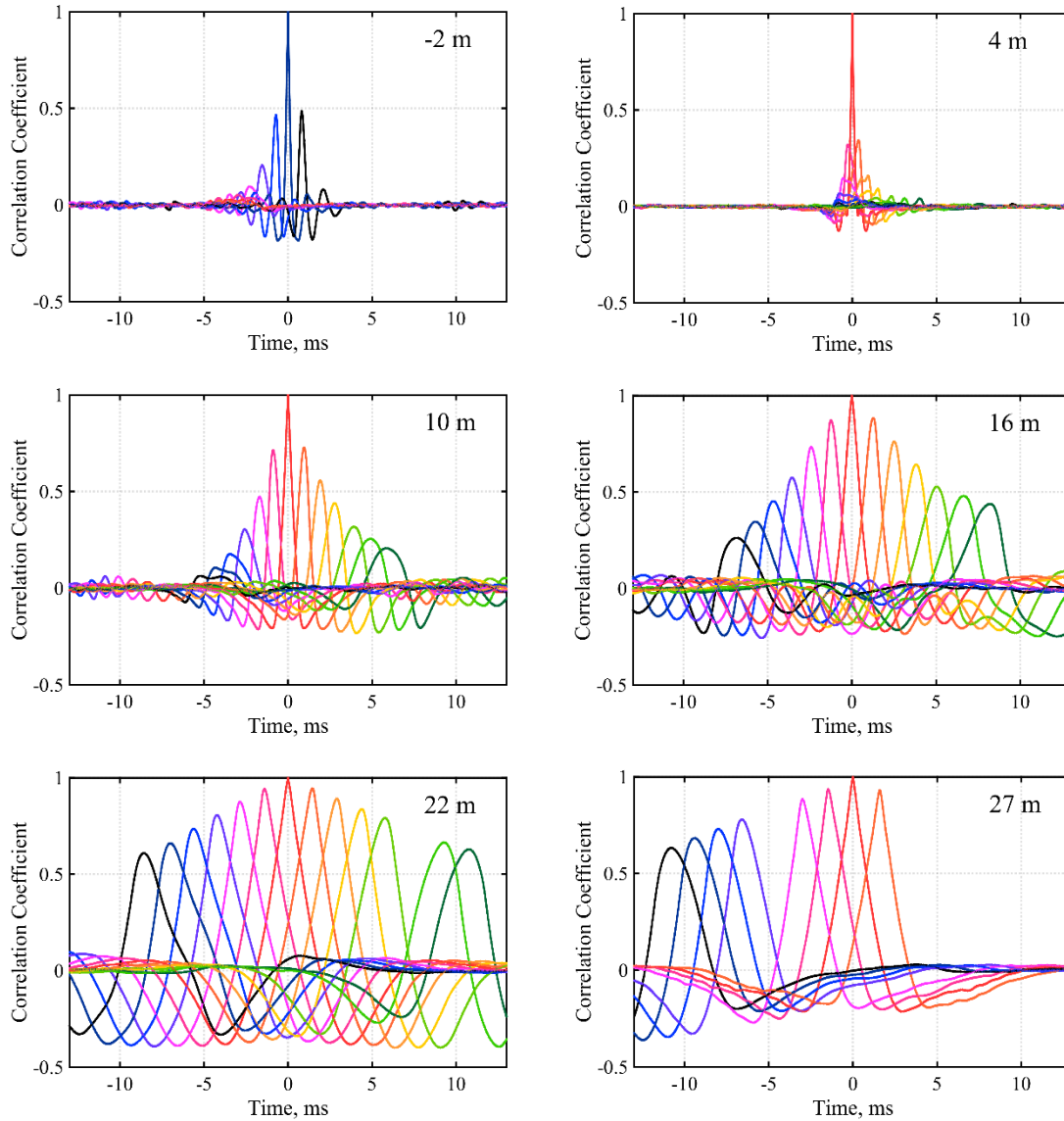
Figure 6. Autocorrelation and neighboring cross-correlation functions of F-22 at Mil power. *Reference microphones along the ground-based array are located at downstream distances of -2, 4, 10, 16, 22, 27 m. Microphone spacing is 0.6 m (2 ft), except for one 1.2 m (4 ft) gap (seen in the bottom two plots).*

While Fig. 6 only shows the cross correlation functions for the 12 microphones closest to the reference microphone, the variation over all 50 microphones can be seen in plots of two-point, space-time correlations known as cross correlograms. As in the case of autocorrelation, the use of the envelope of the Hilbert transform allows the information in the space-time correlation/cross correlograms to be represented on a logarithmic scale, which facilitates the identification of low level features as well. Envelope-based cross correlograms of the envelopes, plotted on a decibel scale ($10 \log_{10} A_{XY}$) for six reference microphones at z_{ref} = -2, 4, 10, 16, 22, and 27 m are shown in Fig. 7 – Fig. 9. The dashed line in each plot indicates the location of the reference microphone. As seen in Fig. 6, the strength and extent of the region of large correlation increases when the reference microphone is placed farther downstream. However, the cross correlograms are significantly different at Int than at Mil and AB. At intermediate power (Fig. 7), significant correlation exists across the entire array. Even at the farthest upstream reference shown, the spatial extent of correlation extends downstream to the end of the array, although it is interesting to note that the correlation is in

11

American Institute of Aeronautics and Astronautics

the form of two secondary lobes and may be the result of engine tones. However, for military (Fig. 8) and afterburner conditions (Fig. 9) the coverage of the high correlation region depends of the location of the reference microphone. When the reference is located at a small downstream distance, i.e. $z_{ref} \leq 5$ m, the extent of significant correlation in space is narrow and grows as z increases. These features indicate the lack of correlation between the upstream radiation and the Mach wave radiation principally directed farther downstream. Another characteristic of the noise that can be seen from the correlograms is an apparent source location. The time of arrival is obtained from the array measurements such that the turning point seen along the line of high correlation is indicative of multiple microphones measuring a source radiating perpendicular to that location. For the intermediate engine condition, the turning point occurs for 0 m $< z <$ 5 m, whereas it occurs at 3 m $< z <$ 8 m for both military and afterburner, regardless of the location of the reference microphone indicating that the overall apparent source regions are at these locations. Cross correlograms were shown for laboratory-scale supersonic unheated and heated jets by Baars *et al.*[22] The primary difference they observed was that the band of high correlation was more linear across the entire array for the unheated than the heated case, in which the slope decreases slightly far from the nozzle. This is similar to the correlograms here for the intermediate case in the $z = 5$-12 m range shown in Fig. 7. Overall, our comparison across three engine conditions with the work of Baars *et al.* corroborates what was noted by Tam and Parrish:[37] the spectral features of the F-22 operated at intermediate power resemble those of a laboratory jet, but that at higher engine powers, noise from high-performance jets contains features not visible in laboratory-scale studies due to the fundamental dissimilarities in the turbulent mixing noise.

There are two additional features of the correlograms that are intriguing because they have not been reported for laboratory-scale jets. First, in many cases, an additional striation appears with relatively low values of correlation that persists over a large spatial aperture. In the $z_{ref} = 10$ m plots at all three engine conditions (middle, left plot in Fig. 7 – Fig. 9), this extra striation is seen as a line with a negative slope that appears to originate at $z \sim 10$ m. A line with similar time delays but a positive slope appears for $z_{ref} < 10$. Because this striation appears at all engine conditions, persists over different run ups with slightly varying strengths, and has a cross correlation similar to that expected for a broadband monopole, it is proposed that this could be a signature of low-level aeroacoustic scrubbing noise as the plume impinges on the ground (see bottom right photo of Fig. 1). The engine nozzle geometry is such that a plume with a shear layer expansion angle of 9° makes contact with the ground at $z \sim 12$ m, making this a plausible explanation. However, further research is needed to verify this hypothesis.

The second feature of interest is the apparent splitting of the high correlation band. The effect is more pronounced at afterburner than at military power and does not appear at intermediate power. For example, at afterburner with $z_{ref} = 16$ m (Fig. 9, middle, right plot), the peak cross-correlation region for values of $z > 22$ m appears to bifurcate far downstream. Reciprocally, for $z_{ref} = 27$ m (bottom right plot), the branching occurs for 10 m $< z <$ 20 m. This branching is significant because the slopes of the two lines likely indicate two different phase speeds corresponding to two noise components with slightly different directivities. This dual directivity has been noted in other studies of high-performance jet noise and exhibits slightly different peak frequencies.[32, 38, 39] In a previous study by Tam and Parrish,[37] it was postulated that one of these sources, the one associated with the peak frequency of 250 Hz, is the result of indirect combustion noise. However, in the correlograms, both branches appear to have roughly the same cusp or turning point at $z_{ref} \sim 5$-10 m downstream, which points to an origin of this second noise component likely being away from the nozzle exit in the vicinity of the dominant mixing noise region. Wall *et al.*[40] have applied acoustical holography to reconstruct the near pressure field back to the shear layer, and they also observe that the origin of the secondary noise component resides farther downstream. While the multiple branches are easily distinguishable at $z_{ref} = 16, 27$ m, the branching is not easily seen in the $z_{ref} = 22$ m reference microphone due to the finite spatial correlation which allows for the resolvable differences in the phase speed.

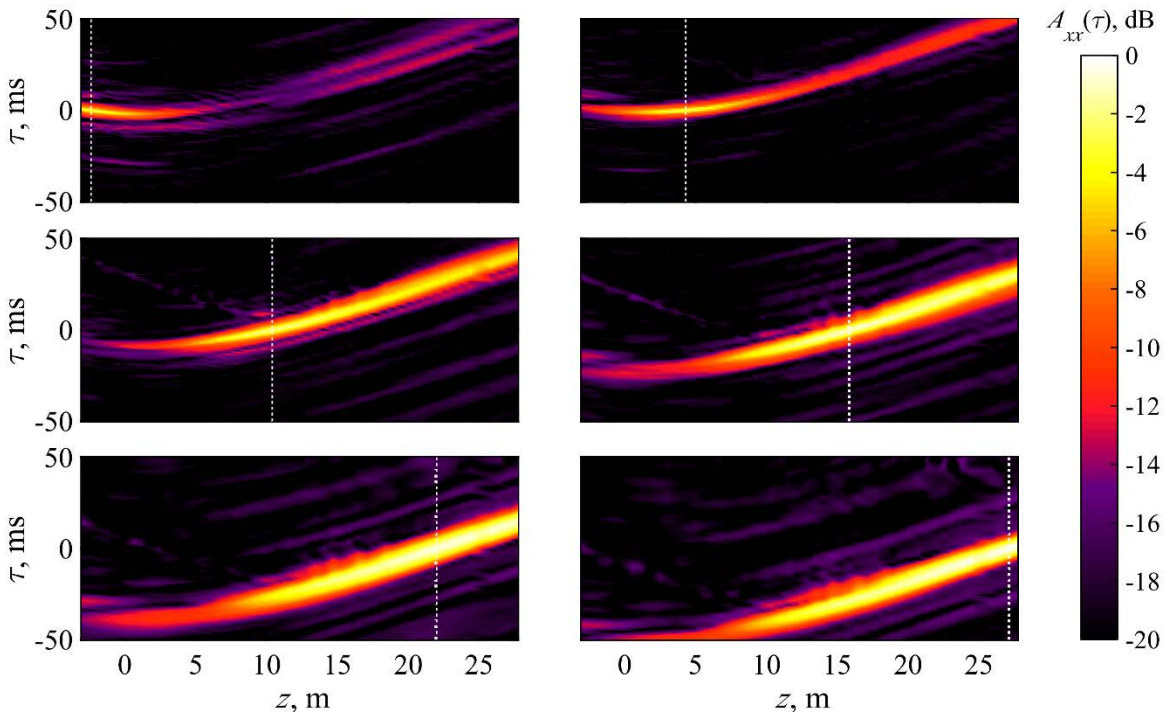American Institute of Aeronautics and Astronautics

Figure 7. Envelope-based cross correlograms at Int. *Envelopes of the Hilbert Transform of the cross correlation between a single mic (dashed white line) and the other 49 microphones along the ground based array at intermediate power (80%).*
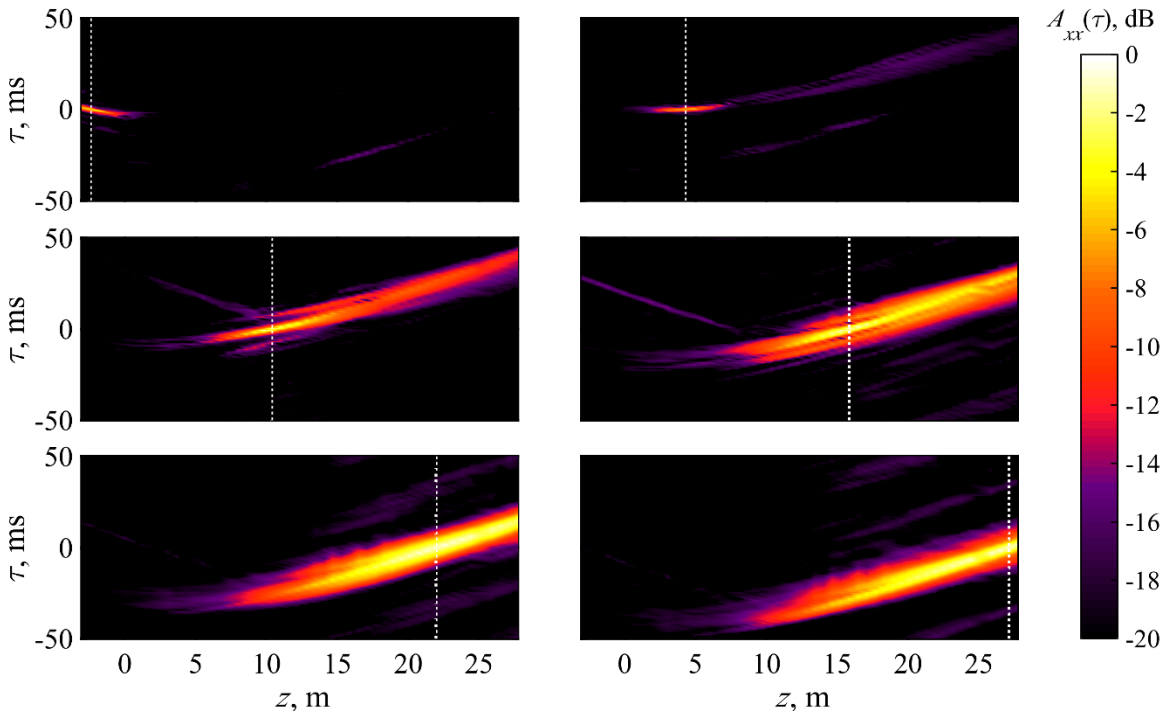
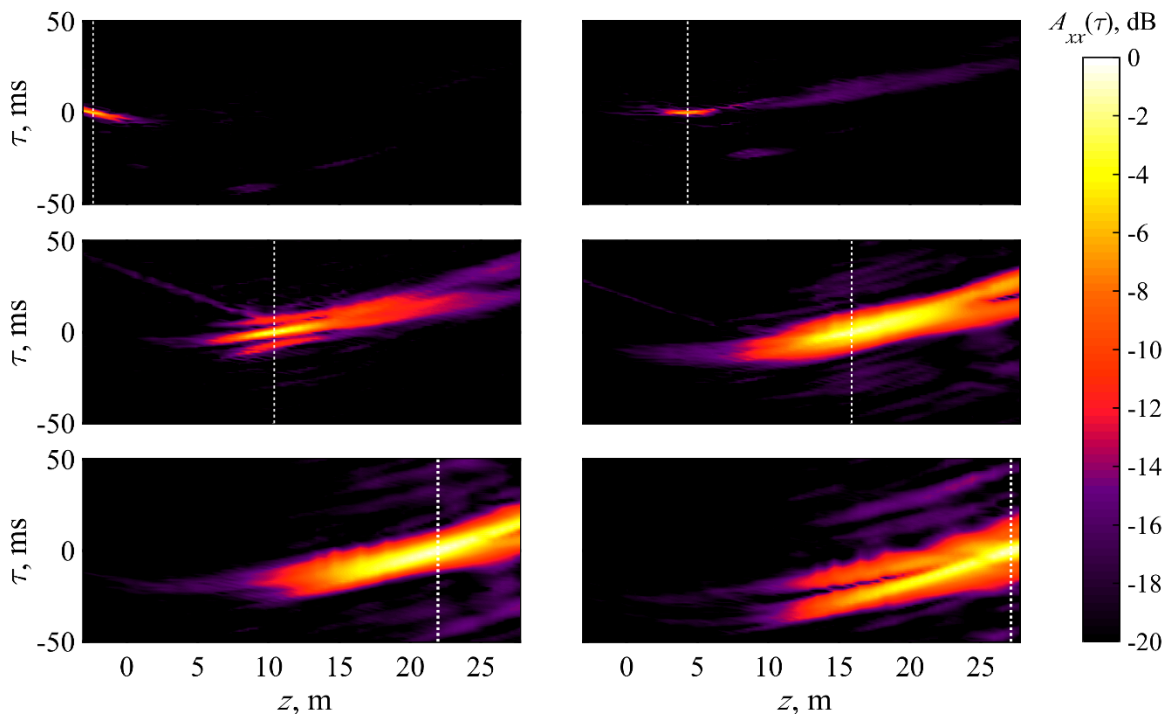**Figure 8. Envelope-based cross correlograms at Mil.** *Similar to Fig. 7 but at military power (100%).*

13

American Institute of Aeronautics and Astronautics

Figure 9. Envelope-based cross correlograms at AB. *Similar to Fig. 7 but at afterburner.*

Phase speed is obtained from the cross-correlation data by expanding on the ability to measure the time of arrival along the array. In this case, the phase speed is estimated as $v_{ph} = \Delta z / \Delta \tau$, where Δz is the distance between microphones and Δt is the temporal delay in the peaks of the cross-correlation. A centered difference based on peak cross-correlation coefficients from three microphones is used to obtain the phase speeds shown in Fig. 10. The dashed line represents the ambient sounds speed, c_0, which is estimated at 347 m/s due to the relatively stable 26.7°C (80°F) temperature during the experiment at Holloman AFB. A positive v_{ph} corresponds to a signal propagating downstream, and negative v_{ph} to upstream propagation, at some angle relative to the array. Thus, when there is rapid change from a negative to positive v_{ph}, the sound is traveling essentially perpendicular to the array, with $v_{ph} = \pm\infty$ and with the sign depending on the look direction up or down the array. The zero crossing is slightly more upstream at intermediate condition (1.2 m < z < 1.8 m) than for military power and afterburner (2.4 m < z < 3.0 m), which are very similar. For large values of z, v_{ph} approaches c_0 indicating that the sound arrival angle relative to a perpendicular is significant. At the far end of the array, the phase speed estimates approach the speed of sound indicating that the sound is traveling at a shallow angle relative to the microphone separation. While this might seem obvious from the geometry, confirmation with the correlation-based phase speed estimate enforces the importance of taking into account end-on effects when processing the data received on these microphones. Unlike a simple delay-sum beamformer which calculates source location based on measurements across the array, this technique calculates source location based on multiple local measurements using only three array elements at a time.
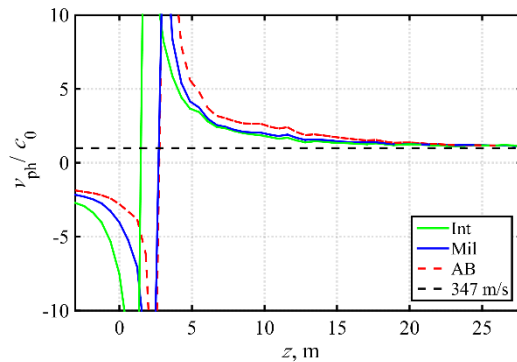
14

Figure 10. Phase speed across ground-based array. *The phase speed is calculated with a centered difference across three microphones, where c_0 is the ambient speed of sound.*

Because the phase speed is the rate at which information travels across the ground array, it is related to the directionality of the sound and thus can be used to estimate the location of the mean noise source. Assuming our sound pressure waves are locally plane-like across three array elements, we can approximate $\sin(\varphi) \approx c_0/v_{\mathrm{ph}}$, where φ is the angle of an arrow pointing from the microphone array back towards the mean noise source. Following this angle back to the jet axis for each microphone gives an indication of the apparent directionality of the jet noise. The results of this phase-speed based ray tracing for the F-22 are shown in Fig. 11. The estimated mean noise source location for the upstream and sideline microphones (-3 m $< z <$ 6 m) are within $z = 2 - 5$ m. Farther downstream ($z > 8$ m) the mean source regions estimated are more spread out and appear to originate from $z \sim 4 - 9$ m. As in the previous analyses, the results for military power and afterburner are similar, slightly downstream and more compact than what is obtained for intermediate power. These estimations for apparent source region are in line with previous estimates obtained from beamforming and intensity analyses,[10, 39] and relate to the spatial variation in spectral content and correlation of the dominant noise field contributions. In future work, band-limited cross correlation analyses would provide arrival angles for frequency-dependent source radiation.
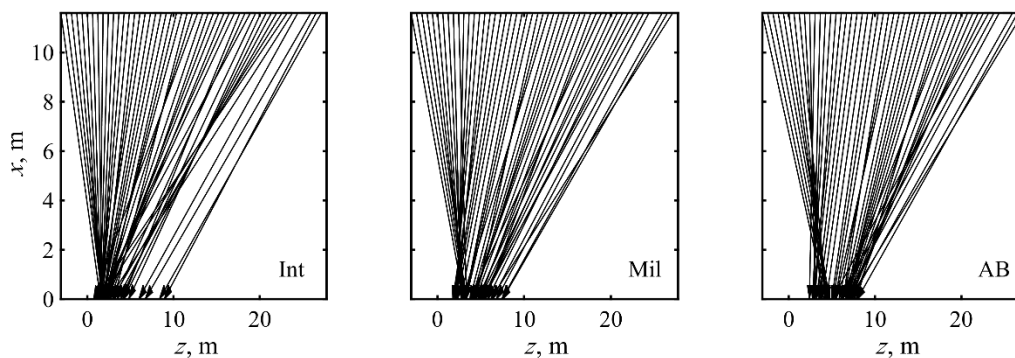

Figure 11. Ray tracing to the jet centerline. *Phase speeds across the 50 microphones calculated locally at the ground array are used to propagate along arrival angles back to the jet centerline at (left) intermediate, (middle) military, and (right) afterburner.*

If the temporal variation is set aside and only peak values of the cross-correlation functions are displayed between pairs of microphones, these peak correlation coefficients provide insight into the spatial variation of the correlations across the array. The peak correlation coefficients for all pairs of microphones are shown at the three engine conditions as contour plots in Fig. 12. It is arranged such that a reference to any two microphone locations provides the cross correlation coefficient (e.g. the diagonal is the autocorrelation coefficient and will be unity by definition). Although the spatial aperture of high correlation is wider overall at intermediate engine condition, clear trends exist across the three engine conditions. To the side of the engine nozzle exit, near $z = 0$ m, the peak correlation coefficients immediately adjacent to a given reference location are nearly negligible at Mil and AB conditions, implying that the distance between neighboring microphones (0.6 m) is larger than the spatial correlation length of the noise in this region. Farther downstream from the F-22 ($z > 10$ m), the spatial region over which there is significant correlation

15

American Institute of Aeronautics and Astronautics

increases significantly, especially for the intermediate engine condition. This increased width implies that relatively longer spatial correlation lengths at downstream distances, as seen in the example Mil cases in Fig. 6. These trends confirm that the nature of noise changes from mostly uncorrelated to the sideline to partially correlated downstream, as has been shown previously for laboratory-scale jets.[1]
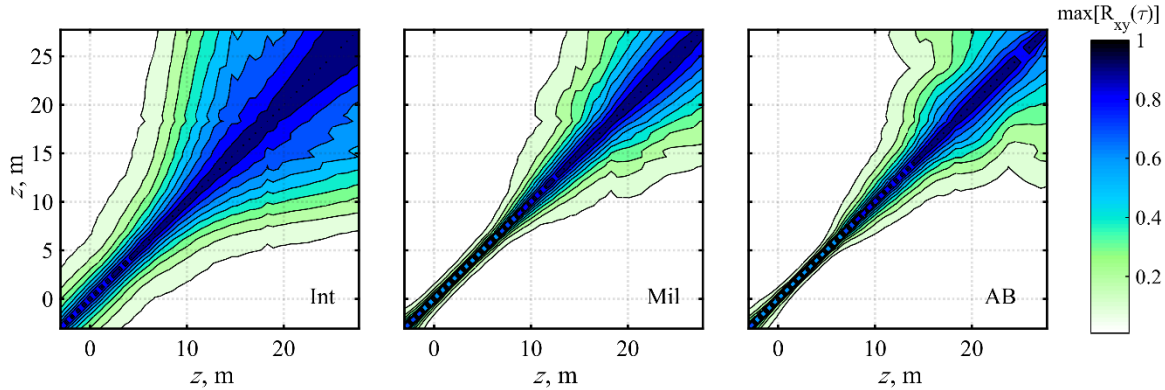

Figure 12. Maximum cross correlation coefficients. *The maximum cross-correlation coefficients are obtained from ground-based array measurements between all 50 microphones for (left) intermediate, (middle) military, and (right) afterburner conditions.*

To effectively measure the distance of significant correlation in the up and downstream directions, length scales based on the maximum cross-correlation coefficients in Fig. 12 are utilized. Using a threshold of $\max(R_{xy}) > 0.5$, the correlation length scales are shown in Fig. 13 for both upstream and downstream cross-correlation measurements. Jet noise to the sideline of the F-22 are, in all three cases, essentially uncorrelated with their neighbors. For the intermediate case, the spatial region over which there is substantial correlation increases rapidly in the downstream direction for $z_{\mathrm{ref}} > 5$ m, indicating a substantial change in the sound field. For example, for $z_{\mathrm{ref}} = 10$ m, the length scale shows that peak cross-correlation values are greater than 0.5 over 3 m in the upstream direction and over 7 m in the downstream direction. The microphone at $z_{\mathrm{ref}} = 13$ m is the last microphone to have both an upstream and downstream distance shown because all microphones in the downstream direction for subsequent microphones have peak correlation coefficients greater than 0.5. Aside from low correlation to the sideline, $z_{\mathrm{ref}} < 7$ m, the length scales for the higher engine powers are substantially different than at intermediate power. Longer correlation lengths occur in the downstream direction, as for intermediate, but the asymmetry between the upstream and downstream lengths is not as great as for intermediate case. At afterburner, there is also the intriguing feature in the correlation lengths between 15 and 20 m where the correlation lengths are much higher than expected by assuming a linear fit. This peak in spatial correlation in the data does not coincide with the maximum radiation region, and while many changes in the spectral content are introduced in the downstream region, most features are also seen in the military engine case. However, one difference between the military and afterburner spectra at this region which was noted by Tam and Parrish[37] is the addition of low-frequency noise which they described as an unknown noise component. The combustion-related "slow wave" they described may be directly related to this phenomenon, although further investigations need to be conducted.
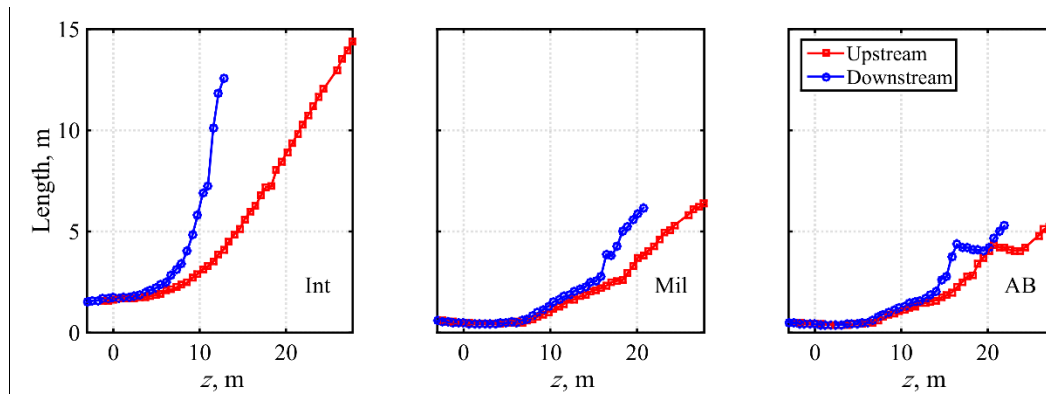
American Institute of Aeronautics and Astronautics

Figure 13. Cross-correlation length measurements. *Distances upstream (red) and downstream (blue) over which the maximum cross correlation coefficient is greater than 0.5 (50%) for intermediate, military, and afterburner.*

The cross-correlation analyses of noise measured on ground-based array of microphones near an F-22 lend insights into the nature of the radiated field and preliminary estimates of the mean source distributions in the jet. Future work in this area centers on improving the characterization of the jet noise sources by striving to find a way to account for the spatial variation in frequency and thus be able to compare correlation calculated for jets of different scales, from laboratory-scale to rockets, and different positions.

B. Coherence Analysis

Because of the spatial variation in spectral shape along the ground-based array at higher engine powers, as displayed in Fig. 2, the coherence is examined to better understand the frequency-dependent features related to the sound field. The coherence between each pair of microphones across the ground array indicates the spatial extent over which sound at a specific frequency is related and allows for an in-depth analysis of the features seen in the cross-correlation. In a manner similar to the correlation analyses, a spatial coherence length, L_{γ^2}, is defined as the length over which there is significant coherence ($\gamma^2 \geq 0.5$). These coherence lengths show effects of different mixing noise contributions in the measurements, including the frequency dependent changes in the coherence lengths to the sideline and farther downstream. In addition, coherence measurements at select frequencies are plotted as a function of measurement location at military engine condition. They highlight both the drop in coherence in the transition region from sideline to downstream radiation as well as the relationship between the dual spectral peaks shown in Fig. 2.

Coherence calculations are made at OTO frequency bands for reference locations $z_{\mathrm{ref}} = -2, 4, 10, 16, 22$ and 28 m along the ground-based array in Fig. 14 – Fig. 16. To the sideline (z_{ref} at -2 m and 4 m), the coherence at all engine conditions is highly symmetric spatially in upstream and downstream directions, with a notable exception below about 50 Hz in the downstream direction. This overall behavior is similar to the cross-correlation results previously shown. At the maximum radiation location on the ground-based array (about 10-25 m at Int, 12 m for Mil and 10 m for AB), the coherence transitions dramatically to be highly coherent at most frequencies below 400 Hz in the downstream direction, although this does not extend in the upstream direction. Thus, for example, the coherence lengths at intermediate condition for $z_{\mathrm{ref}} = 10$ m extend up to 10 m in the downstream direction, but only about 4 m in the upstream direction. Note that in the higher frequency range ($f > 500$ Hz), the coherence is much more symmetric in space. Military and afterburner cases share similar general features with intermediate, except that L_{γ^2} values progressively decrease as the engine power increases. They also include a region of unusually low coherence at $z = 10$ m, which is noticeable in the $z_{ref} = 6$ m plot, and warrants further investigation. The distinguishing features in the spatial dependence of coherence length across engine conditions are few: 1) the onset of high L_{γ^2} values at afterburner occurs slightly upstream compared to military—which occurs upstream of the intermediate case—consistent with the idea that coherent Mach waves are shifting upstream with the increase in engine power,[30] 2) at $z_{\mathrm{ref}} = 22$ m the coherence at 100 Hz is markedly low at afterburner for unknown reasons, 3) coherence in the military case at $z_{\mathrm{ref}} = 22$ m is slightly lower at 200 Hz and then slightly higher the 300-500 Hz range, although this effect is only seen at values $\gamma^2 < 0.4$. It is believed that this effect is related to the presence of multiple spectral peaks at this measurement location.
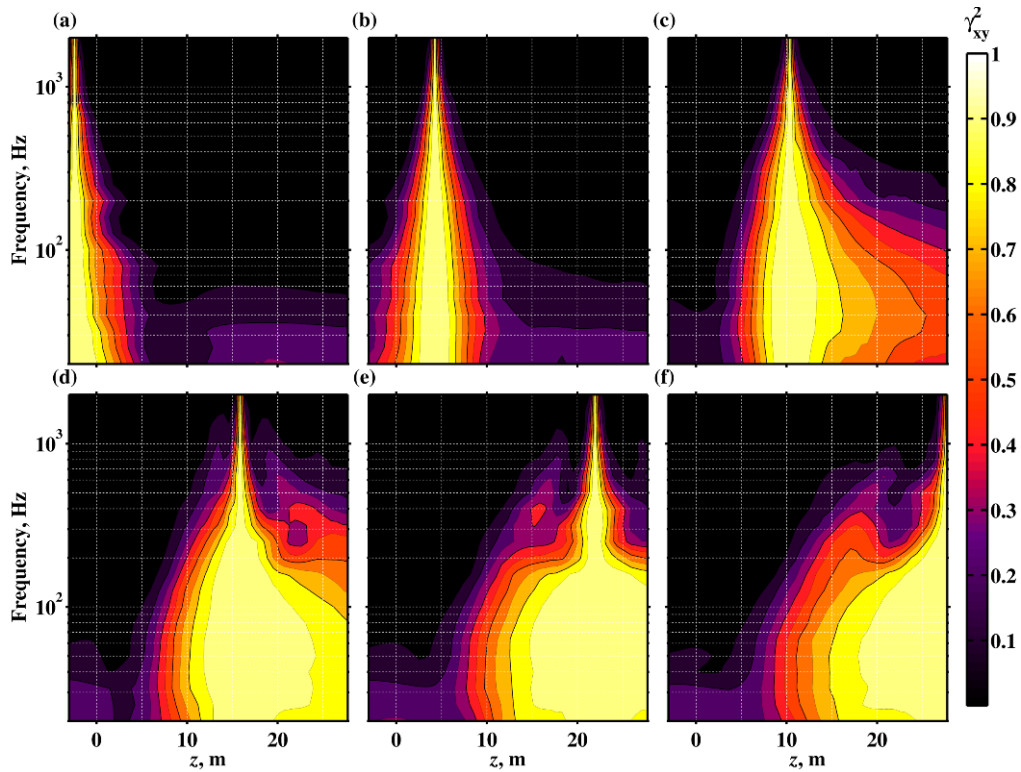
American Institute of Aeronautics and Astronautics

Figure 14. Coherence values across the ground-based array for select references at Int. *Coherence values calculated for intermediate engine condition (80%) relative to six reference microphones at (a) -2 m, (b) 4 m, (c) 10.4 m, (d) 16 m, (e) 22 m, (f) 28 m. Solid contour lines are incremented by 0.2.*
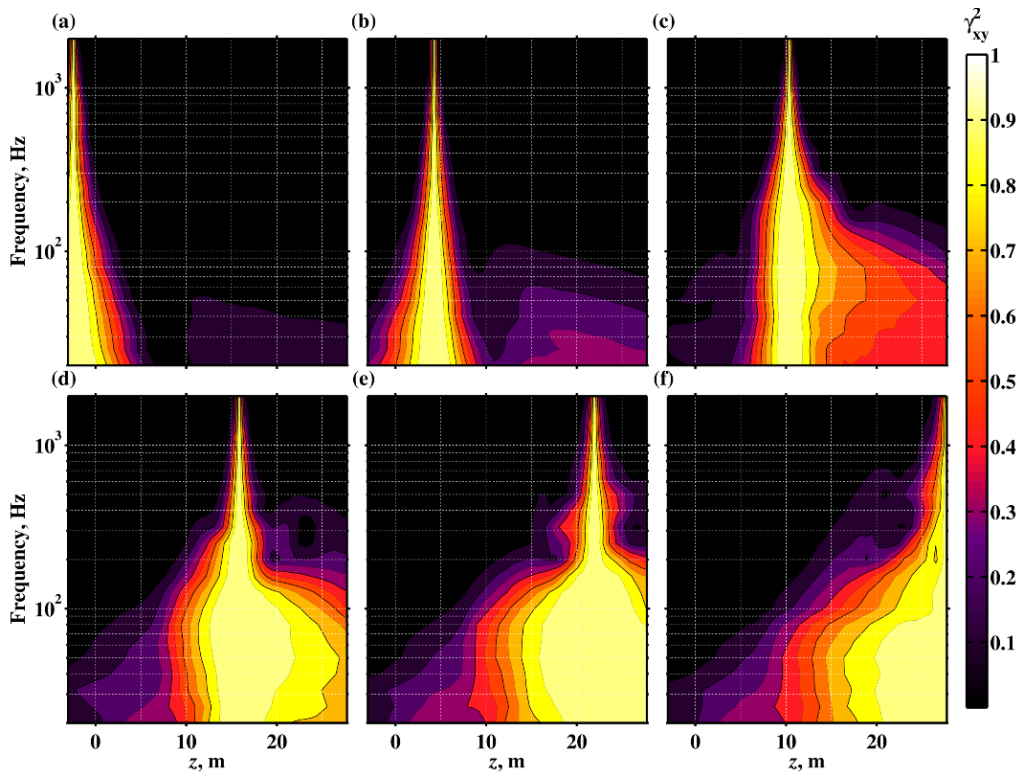

Figure 15. Coherence values across the ground-based array for select references at Mil. *Similar to Fig. 14, except at military power (100%).*

18

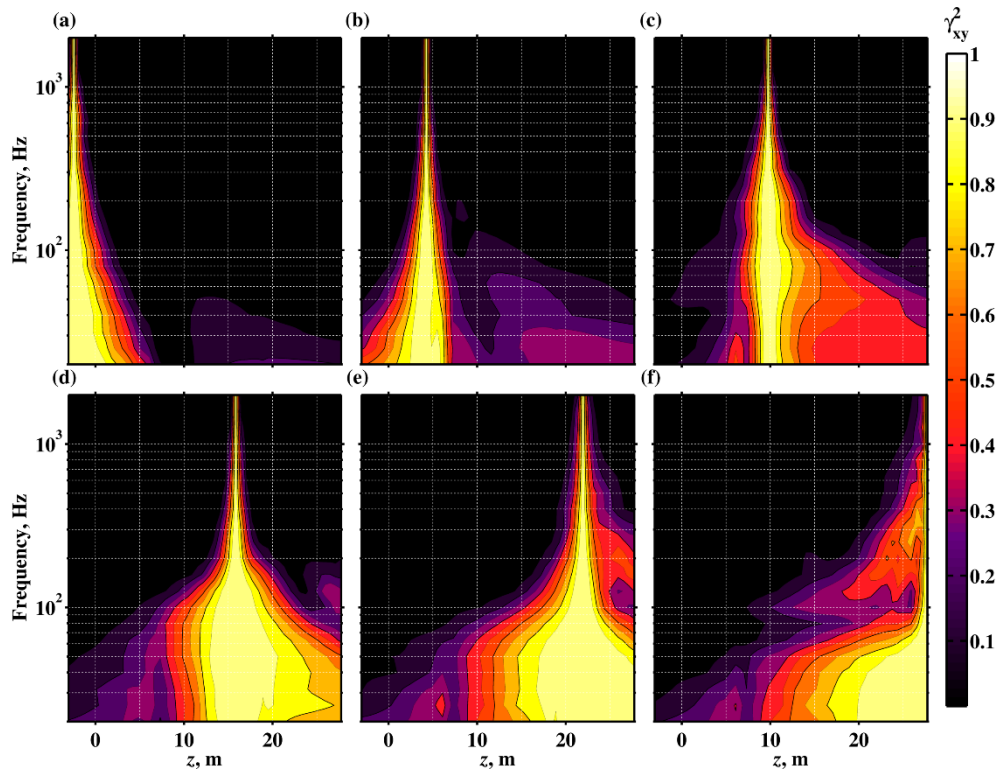American Institute of Aeronautics and Astronautics

Figure 16. Coherence values across the ground-based array for select references at AB. *Similar to Fig. 14, except at afterburner.*

These spatial coherence lengths are quantified and calculated to quantify the spatial and frequency-dependent variation in the coherence of the sound field. As the coherence was shown previously to exhibit a high degree of asymmetry, we separate the coherence length into two pieces to show both an upstream coherence length, $L_{\gamma^2}^-$, and a downstream coherence length, $L_{\gamma^2}^+$, where upstream describes positions closer to the nozzle exit than the reference microphone, and downstream is farther away. These coherence lengths are shown in Fig. 17 for the three engine conditions with $L_{\gamma^2}^-$ values on the top row and $L_{\gamma^2}^+$ below. As seen in the previous figures, coherence lengths generally decrease with increasing engine condition. In addition, coherence lengths for most distance/frequency combinations are largest in the downstream direction where large-scale structure turbulent mixing noise dominates. To the sideline, upstream and downstream coherence lengths are similar in value, which is likely tied to the presence of fairly omnidirectional radiation to the sideline, as described by many previous studies, and may be related to noise generated by fine-scale turbulent structures with short spatial coherence lengths. As z_{ref} is increased, it can be seen that downstream coherence lengths increase more rapidly than upstream coherence lengths, particularly for frequencies $f < 200$ Hz, because of the asymmetrically-shaped coherence measurements in Fig. 14 – Fig. 16. For example, at 100 Hz and $z_{\text{ref}} = 10$ m at Int, $L_{\gamma^2}^- \sim 6$ m, whereas $L_{\gamma^2}^+ \sim 10$ m. Due to the way the coherence length is calculated, good estimates of upstream and downstream coherence lengths are not available when the array does not extend sufficiently far to capture the location at which $\gamma^2(x, f) \leq 0.5$, and these regions are indicated by gray in the figure.

The coherence lengths shown in Fig. 17 can also highlight and characterize particular features in sound field. For example, for all engine conditions, the variation in $L_{\gamma^2}^+$ is seen to be very pronounced for $f < 200$ Hz and changes rapidly in the $z_{\text{ref}} = 10 - 12$ m range. This corresponds to the regions where the maximum overall levels occur, as shown in Fig. 1, and where the spectral shapes are well described by solely the large-scale turbulent structure similarity spectrum in Neilsen *et al.*[31] In addition, in the military and afterburner cases, a small increase in $L_{\gamma^2}^-$ and $L_{\gamma^2}^+$ is visible, between 125 Hz $< f <$ 300 Hz at Mil and 125 Hz $< f <$ 400 Hz at AB, and which is slightly asymmetric (e.g. high $L_{\gamma^2}^+$ values from $z = 9 - 10$ m, high $L_{\gamma^2}^-$ values from $z = 11 - 12$ m for AB case). Considering spectral levels in Fig. 2, this corresponds to the dominant spectral features across the array between $200 < f < 500$ Hz. Thus, the coherence lengths of the primary radiation at these frequencies are significant, although much lower when compared with the

American Institute of Aeronautics and Astronautics

radiation that is farther downstream and which radiates with a peak frequency of about 125 Hz. A transition region is also shown to exist where values of both $L_{\gamma^2}^{-}$ and $L_{\gamma^2}^{+}$ indicate a dip in coherence lengths. For both Mil and AB, this dip occurs for 40 Hz < f < 125 Hz and at $z_{ref} \sim$7-8 m for $L_{\gamma^2}^{-}$ and at $z_{ref} \sim$5-6 m for $L_{\gamma^2}^{+}$, dependent on frequency. Near these locations, Neilsen *et al.*[31] showed that a combination of the fine-scale and large-scale similarity spectra is necessary to represent the measured spectra. In addition, the frequencies at which the dip in coherence length occurs coincides with the locations where the two spectra are equal contributors to the spectral levels. This effect is further explained in the following paragraph. There is also a region of very low coherence lengths in the AB case for f < 50 Hz at $z = 8 - 10$ m, although whether this is physical or a processing artifact is under investigation.
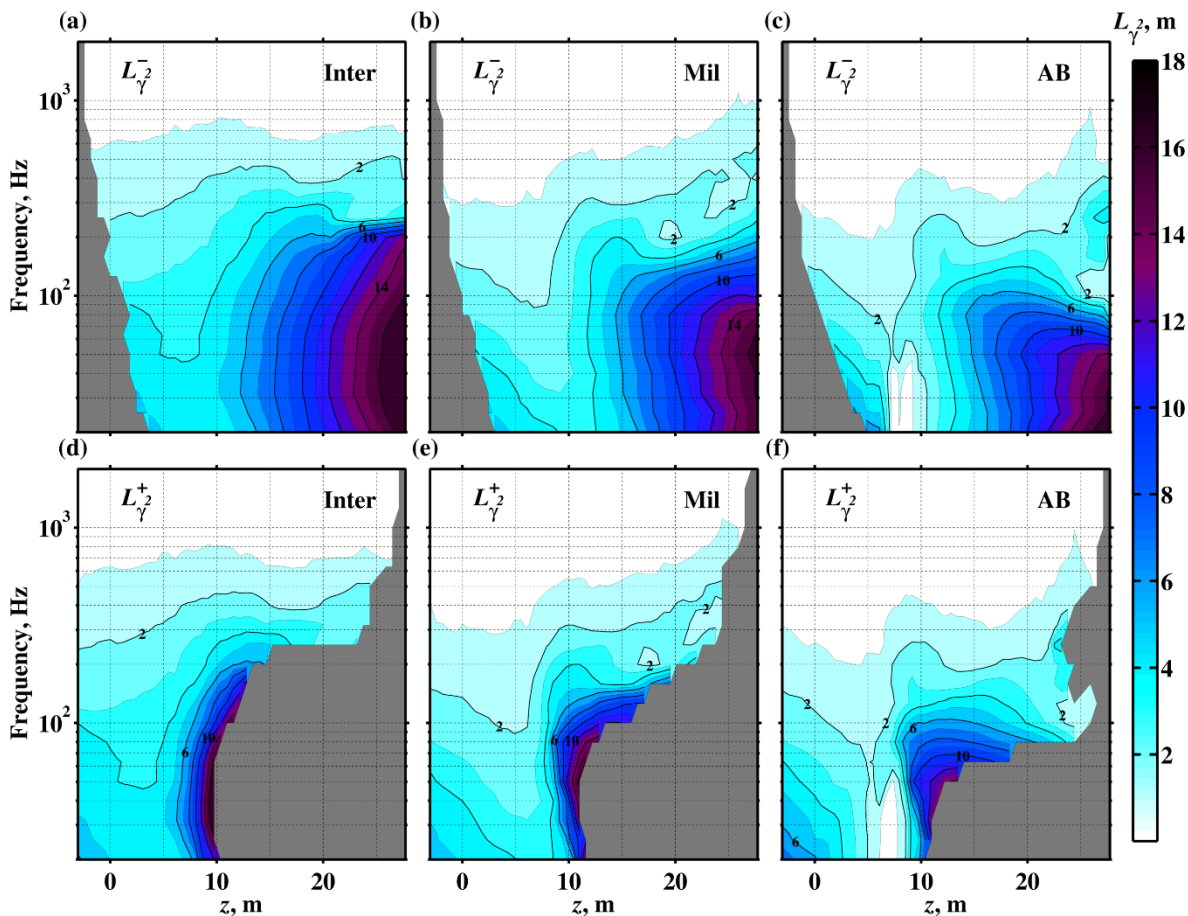

Figure 17. Spatial coherence lengths in the upstream and downstream direction. *Upstream coherence lengths, $L_{\gamma^2}^{-}$, in (a)-(c) and downstream lengths, $L_{\gamma^2}^{+}$, in (d)-(f) for Int (left), Mil (middle) and AB (right). Contour colors are spaced at 1 m increments with solid lines at 2 m increments. Grayed out portions are areas where the array aperture was insufficient to calculate the coherence length.*

To further investigate the spatial variation in the low-frequency coherence lengths, we examine the coherence at three particular frequencies between all microphones on the ground-based array for the military engine case in Fig. 18. Coherence plots are oriented such that self-coherence (nominally unity) occurs along the diagonal, and coherence between two distinct locations can be found along the off-diagonal elements. Shown below the coherence maps are the corresponding sound pressure levels across the array at each frequency. The largest levels generally correspond to locations with the longest coherence lengths. However, this does not seem to be the case in the upstream direction. At 50 Hz, a narrower spatial extent of significant correlation is located at $z = 7.5$ m, separating larger coherence lengths in the far downstream and the upstream direction. This is also present at 100 Hz and also 200 Hz, although more difficult to observe. In this region, the SPL increases with z, but the coherence lengths unexpectedly decrease to a minimum value. Two possible explanations are under investigation. First, the mean source region may exist at this location along the jet such that the minimum coherence length corresponds to the infinite phase-speed across the array.

20

American Institute of Aeronautics and Astronautics

In this case, coherence lengths would be greatest at the extreme distances from the source along the array, which contradicts the measured coherence where the regions of high coherences do not necessarily correspond to the largest z values. Furthermore, the source region at Mil condition and 50 Hz was observed through intensity measurements and holography results to be about 8-12 m downstream.[38, 39] Alternatively, the minimum coherence levels may result from the interference of competing independent sources. Neilsen *et al.*[31] showed that the spectral shapes along the ground-based array change from matching the general features of the fine-scale similarity spectrum to those of the large-scale similarity spectrum over a transition (or combination) region that occurs over $z = 6 - 8$ m for frequencies below 400 Hz. Although there is some latitude in shifting the similarity spectra to match the data, the presence of similar levels of the independent fine-scale and large-scale turbulent mixing noise would account for the drop in coherence in this transition region. Thus, the independent signals would be responsible for increasing overall levels and yet decreasing coherence lengths in this region. While some have recently discounted the two-source model of jet noise[1, 41] in favor of continuous source models, such as a wavepacket ansatz, the fit performed independently by Neilsen *et al.* nevertheless explains the otherwise discrepant effects seen here.

The coherence at 200 Hz also shows evidence related to the dual-spectral peaks at this engine condition. While the spatial variation in coherence at 50 and 100 Hz appear to be scaled versions of one another, the coherence map at 200 Hz has a fundamentally different shape: the region of large coherence does not continue to grow for $z > 10$ m. Instead, there is an additional narrowing of the correlation lengths for 15 m $< z <$ 20 m. In the cross-correlation measurements shown above, the envelope-based cross correlograms showed splitting in the downstream measurements, corresponding to radiating sources with different directivities. This is related to the dual spectral peaks which are seen in Fig. 2 and in the levels in Fig. 18(f), which radiate to different downstream locations at the measurement array as seen by the secondary rise in level for $z > 20$ m. While these two features are relatively self-coherent, coherence between the two peaks is only minimally significant. These radiators may thus be independent and associated with two incoherent sources. This is explored in greater detail in Ref. [38].
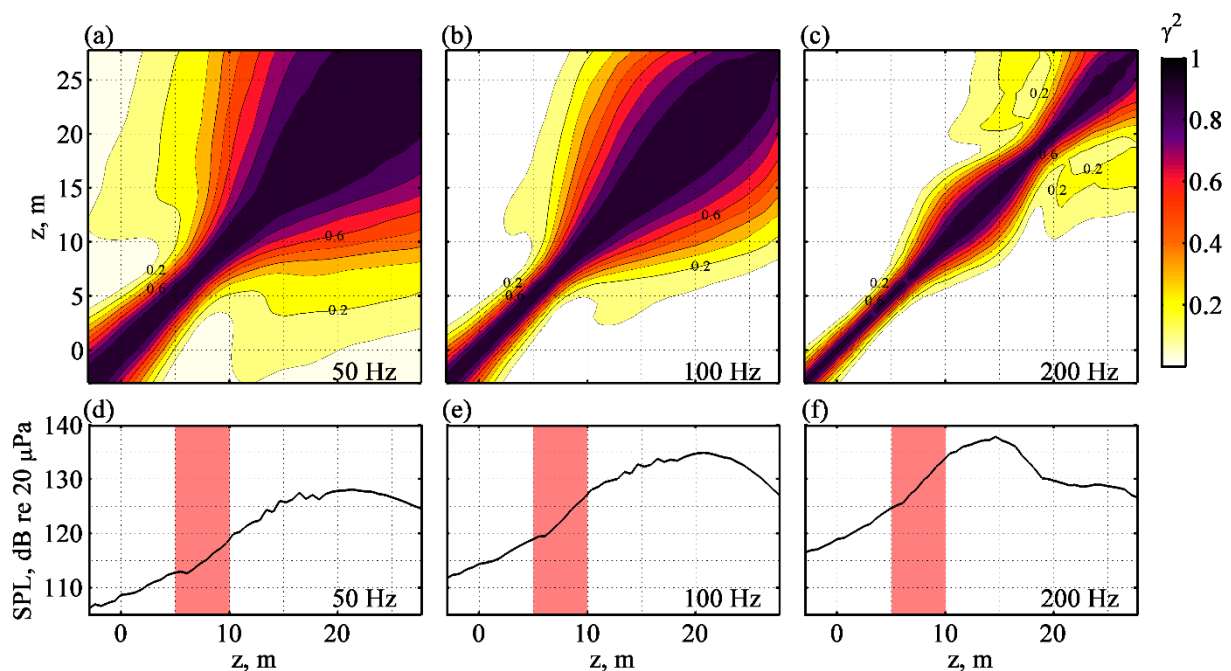

Figure 18. Spatial coherence for select one-third octave band center frequencies at Mil. *Coherence values across the ground-based array as a function of position at military power for (a) 50 Hz (b) 100 Hz (c) 200 Hz. Corresponding sound pressure level measurements across the array at respective one-third octave frequencies are shown in (d)-(f).*

C. Source Coherence Analysis

The previous analyses in this paper deal with defining the correlation and coherence properties of the radiated sound field. In this section, estimates of the source coherence are obtained by beamforming the pressure measurements obtained at the ground-based array to the jet centerline, and the results are evaluated in light of what has been learned

American Institute of Aeronautics and Astronautics

about the field coherence. A DAMAS-C processing algorithm provides an estimate of the equivalent source distribution, the self-coherence, and equivalent source coherence lengths. The term equivalent source is used because the DAMAS-C results are linked solely to the acoustical properties of the jet noise and not the flow properties in the jet. Because the DAMAS-C algorithm makes no assumptions on the degree of source correlation that exists within the scanning region, the source coherence can be measured as a byproduct of the analysis. The DAMAS-C methods described in Section II produce deconvolved beamforming results of the pressure measurements due to the combination of two simultaneous measurement locations along the jet centerline. These results are shown in Fig. 19 for frequencies of 100, 200 and 315 Hz at each engine condition. A given diagonal element of each two-dimensional plot shows the beamforming response for a single measurement location (as is typically calculated in beamforming algorithms), and an off-diagonal element represents the cross-levels for two simultaneous beamforming locations. These represent equivalent source maps for all engine conditions that show extended source distributions that shrink in size and in cross-level with increasing frequency. In addition, the location of the peak source level moves farther downstream with increasing engine condition.
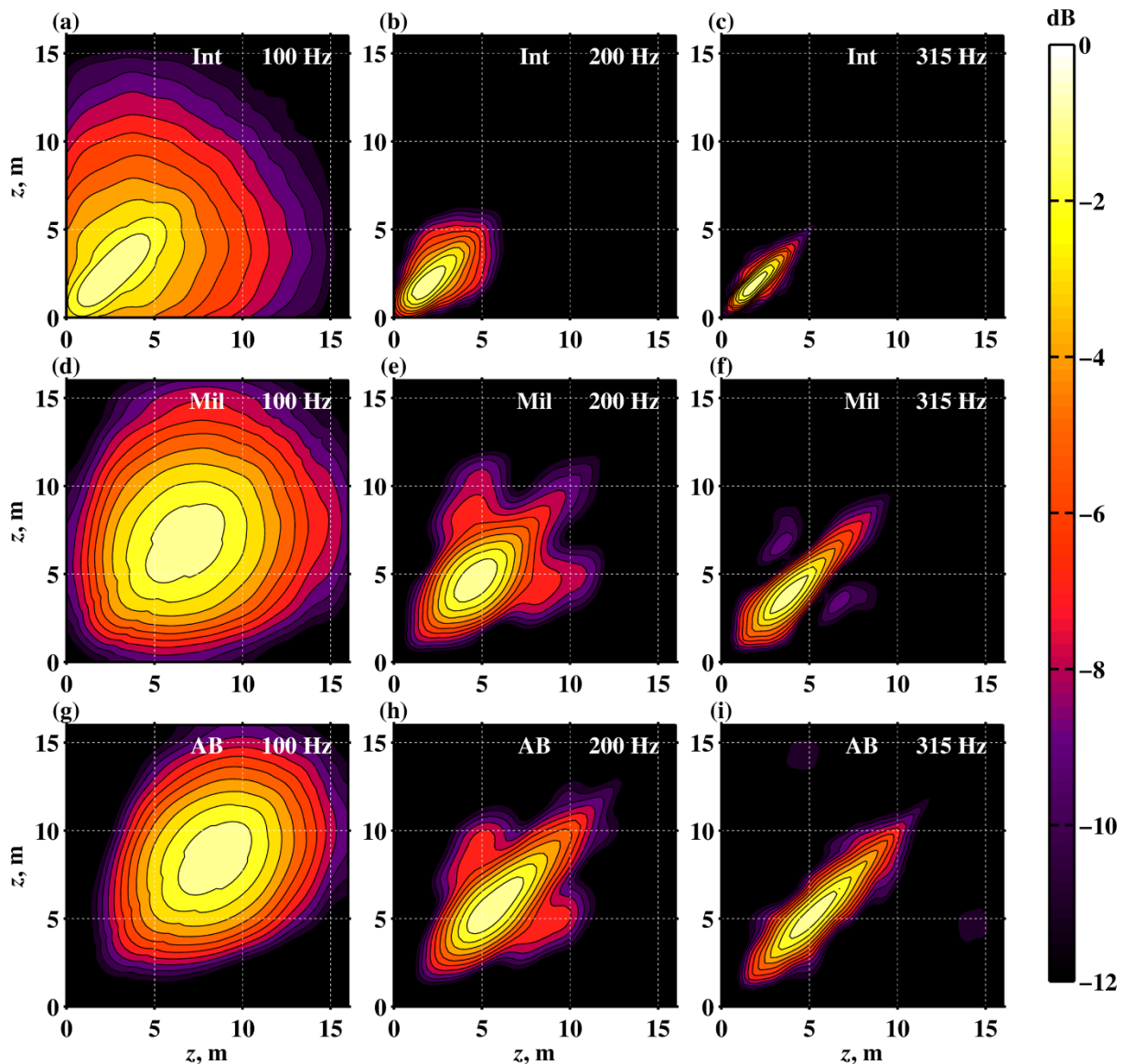

Figure 19. Equivalent Source Levels from DAMAS-C. *The levels of the equivalent source distributions reconstructed by DAMAS-C to the jet centerline, based on the 50-microphone ground-based array near the F-22 at (top) Int, (middle) Mil, and (bottom) AB for frequencies (left) 100 Hz, (center) 200 Hz and (right) 315 Hz. The*

American Institute of Aeronautics and Astronautics

horizontal and vertical axes are in meters, and the color represents level relative to the peak value at that frequency and condition, incremented at intervals of 1 dB.

To calculate the coherence across the source distribution, we normalize the off-diagonal elements of each plot using the corresponding diagonal values to produce source coherence maps shown in Fig. 20. The diagonal elements of each figure represent the self-coherence, for a single reconstruction location, which by definition is unity. The off-diagonal elements, $\gamma^2_{z_1 z_2}$, represent the coherence between equivalent sources located at positions z_1 and z_2 along the jet centerline. To reduce the processing artifacts introduced when coherence is calculated from low-level beamforming results, a threshold of 12 dB below the peak source reconstruction level was chosen such that coherence values below this threshold were grayed out. The source coherence contracts with increasing frequency, similar to the trends seen in the DAMAS-C levels. The spatial aperture of significant coherence at 100 Hz are particularly large at all engine conditions, with source coherence lengths, $\gamma^2 > 0.5$, that span up to 5-6 m for Mil and AB cases at the peak level regions. Unlike the field coherence lengths from the ground-based array measurements, the source coherence lengths do not vary as widely across engine conditions. However, an interesting observation is seen in the 200 Hz coherence measurements at military condition: there is significant (0.2 – 0.3) coherence between the source distributions at 5 m and with locations farther downstream, up to the 10 m location. This is also seen to a lesser degree in the afterburner case. Because these regions of high coherence also mark the maximum source region, it is possible that the relatively high levels in this region produce processing artifacts seen as off-diagonal measurements. The 315 Hz DAMAS-C levels at Mil also show higher levels corresponding to the peak source location, however, the levels are much lower and do not appear in the coherence measurements. If the features are indeed physical, one explanation is that the primary source distribution contains some significant degree of correlation which extends throughout the source region. This would be evidence for a wavepacket-like model of jet noise which assumes each wavepacket to be self-coherent along the source distribution region. In addition, there appears to be a region between the 5 m and 10 m locations where coherence drops. For this engine condition and frequency, Wall *et al.*[38] have used holography methods to show the reconstructed sound field which contains two lobes, each with a distinct directivity, that coalesce at about 7 m along the jet centerline. The effect of an independent radiator in this region would be to mask the long self-coherence of a more generally distributed primary source. The occurrence of two lobes in the far-field data, discussed in both the cross-correlation and coherence analyses, supports a theory of two independent sources radiating with different, distinct directivities towards the ground-based array. While much has yet to be done towards a more conclusive theory, further investigation may better support a relation between the dual-directivity in the field and the source coherence from the DAMAS-C measurements.
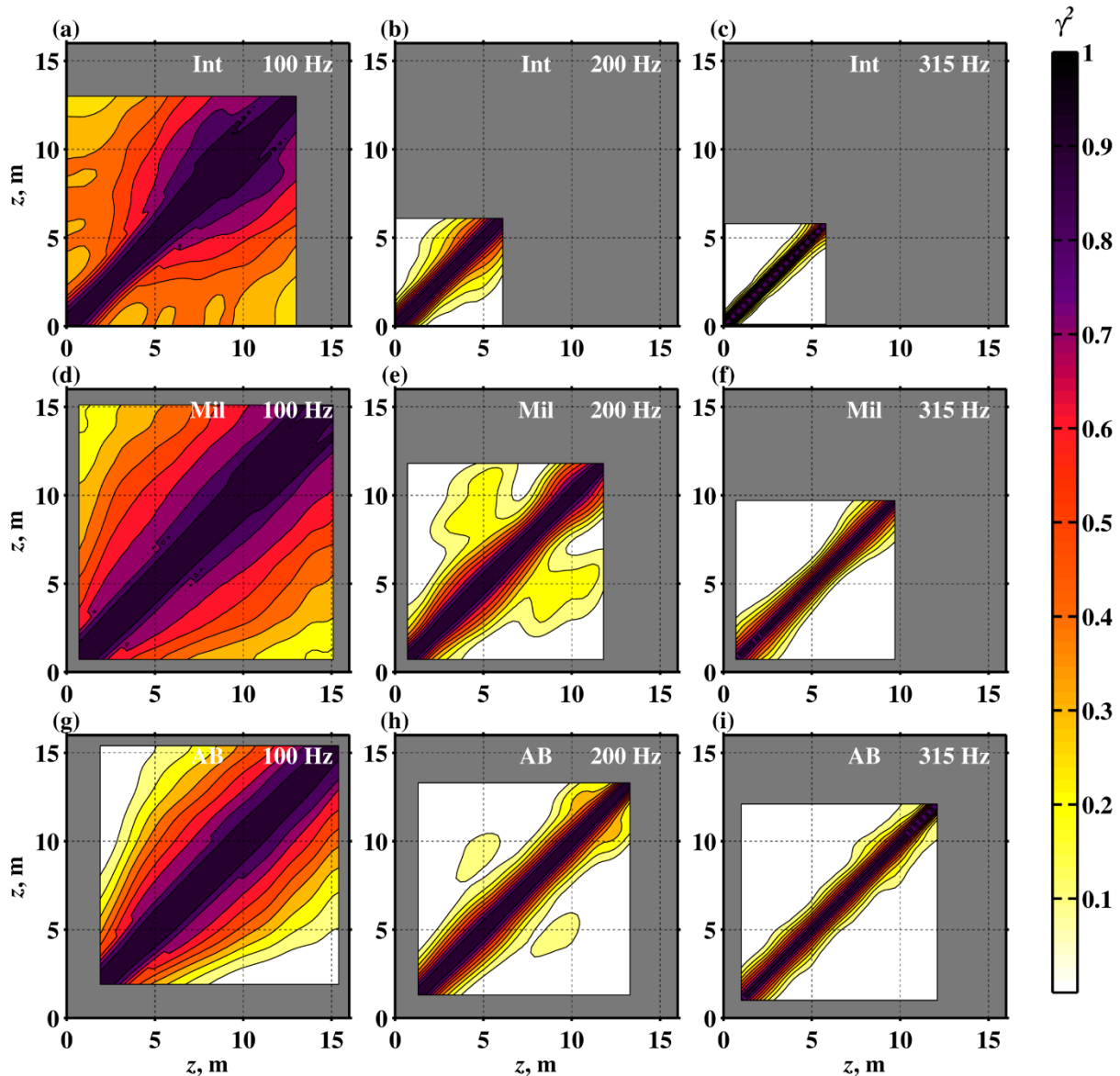
American Institute of Aeronautics and Astronautics

Figure 20. Equivalent Source Coherence from DAMAS-C. *The coherence of the corresponding equivalent sources reconstructed by DAMAS-C as shown in Fig. 19. The horizontal and vertical axes are in meters, and the color represents coherence level, incremented at intervals of 0.1. Grayed out regions represent regions not displayed of the coherence where the maximum corresponding source levels (along the diagonal) were below 12 dB from the peak level.*

V. Conclusion

Correlation measurements have been presented from ground-array data collected in the near field of a tethered F-22A at intermediate, military and afterburner engine conditions. A fundamental difference exists between single-point correlation measurements within and outside the Mach wave radiation region. It was found that temporal scales from single-point measurements show larger values downstream, even when scaled by the peak frequency at each measurement location. Deep negative loops are prevalent in the downstream direction, indicative of large-scale structures. However, a secondary set of negative loops is seen in single point measurements at certain downstream locations, which has not been observed in laboratory-scale studies. Negative loops are also found in the sideline measurements, which may be indicative of broadband shock-associated noise. Many of these features are more readily visible through an autocorrelation envelope, via the Hilbert transform, which aids in discerning low-level features and provides a consistent means of measuring temporal correlation scales.

American Institute of Aeronautics and Astronautics

In the two-point correlation measurements, spatial as well as temporal analyses on the radiation field provide insight into the acoustic sources at each engine condition. As seen on similar lab-scale studies, the spatial decay of correlation is greatest at the sideline whereas the downstream correlation measurements are highly correlated in space and time. However, the military and afterburner engine cases show distinctly different single-point (auto) and two-point (cross) space-time correlation functions compared to results at intermediate power, which are more similar to studies reported for laboratory-scale jets.[1, 4] These features at high engine powers help to characterize the properties of the maximum radiation region, where there is a discrete transition in level between two peak frequencies,[32] a phenomenon not found in laboratory-scale data. A transition region also exists along the measurement array where correlation measurements are highly correlated in the downstream direction only, signaling the onset of large-scale structure related noise. Envelope-based correlogram measurements allow for low-level correlation feature analysis and reveal that, unlike at military and afterburner, the intermediate engine condition showed appreciable correlation across the entire array. Furthermore, events in the downstream correlogram measurements correspond to multiple phase-speeds at military and afterburner. This is indicative of multiple radiating sources with distinct directivity patterns. In each case, the correlograms show turning points, which are used to estimate the downstream distance at which the radiation propagation was perpendicular to the array. In addition, the time of arrival seen in the correlogram measurements are used to calculate the phase speed across the array as well as the angle of arrival. These angles are ray-traced to the jet centerline as another means of estimating the mean source location, and results agree with beamforming and similar source reconstruction methods.

Coherence measurements provide for frequency-dependent spatial scales over which source mechanisms extend to the radiation properties. Coherence lengths at each engine condition have been shown to be highly asymmetric, due to the directional nature of the large-scale structures and rapid onset of the Mach wave radiation region. Within this region, coherence lengths spanning multiple acoustic wavelengths are observed below 400 Hz, while outside this region the coherence lengths are generally lower and proportional to frequency. In addition, signs of mixing between sideline and downstream radiation exist, marked by low coherence values which separate the sideline and downstream radiation. These areas of low coherence agree with results from Nielsen *et al.*[31] that show the radiation in this region to contain equal contributions from both fine-scale and large-scale noise. Additionally, equivalent source coherence lengths, derived from beamforming measurements using ground-based array data, have been calculated using the DAMAS-C algorithm. Beamforming measurements steered to the jet centerline show large extended sources which decrease in size with increasing frequency. Comparing three frequencies at each engine condition, it was found that the self-coherence across these sources was greatest at 100 Hz, and coherence dropped steadily with increasing frequency. However, a region of particularly low coherence was found in the data at 200 Hz, corresponding to the frequency where two lobes with different directivities exist are believed to coalesce at the source region, although further investigation is required to understand a possible relation between these observations. Future beamforming measurements from solely large-scale structure dominated array measurements may show results that reveal different source coherence features.

Understanding the different independent mechanisms within the jet noise radiation is aided by correlation analyses, making them fundamental in the continued development of more complete jet noise models. For example, accurate source models, e.g. wavepacket models, should satisfy the coherence and correlation properties of the field in addition to spectral and overall levels. Currently, some wavepacket models that do fairly well in representing the measured spectral properties assume a single self-coherent source and thus do not accurately represent the correlation properties observed. Therefore, incorporation of the correlation properties of the field will produce models that are more physically accurate. In addition, because correlation affects overall levels, jet noise reduction strategies are enhanced when source correlation properties are considered. The cumulative results of these investigations provide a deeper understanding of jet noise source features and provide a full-scale military jet noise benchmark that should be considered when evaluating laboratory-scale jet studies and computational simulations of jet noise.

Acknowledgments

American Institute of Aeronautics and Astronautics

U.S. Department of Energy and USAFRL. Distribution A: Approved for public release; distribution unlimited. 88ABW Cleared 04/23/2015; 88ABW-2015-2059.

References

[1] C. K. W. Tam, K. Viswanathan, K. K. Ahuja, and J. Panda, "The sources of jet noise: Experimental evidence," *Journal of Fluid Mechanics* **615**, 253-292 (2008).

[2] C. K. Tam, N. N. Pastouchenko, and K. Viswanathan, "Continuation of the Near Acoustic Field of a Jet to the Far Field. Part I: Theory," AIAA Paper 2010-3728, 2010.

[3] C. K. W. Tam, K. Viswanathan, N. N. Pastouchenko, and B. Tam, "Continuation of Near-Acoustic Fields of Jets to the Far Field: Part II Experimental Validation and Noise Source Characteristics," AIAA Paper 2010-3729, 2010.

[4] K. Viswanathan, J. R. Underbrink, and L. Brusniak, "Space-time correlation measurements in near fields of jets," *AIAA Journal* **49**, 1577-1599 (2011).

[5] B. M. Harker, K. L. Gee, T. B. Neilsen, A. T. Wall, S. A. McInerny, and M. M. James, "On autocorrelation analysis of jet noise," *Journal of the Acoustical Society of America* **133**, EL458-EL464 (2013).

[6] A. T. Wall, M. D. Gardner, K. L. Gee, and T. B. Neilsen, "Coherence length as a figure of merit in multireference near-field acoustical holographya)," *Journal of the Acoustical Society of America* **132**, EL215-EL221 (2012).

[7] A. Michalke, "On the effect of spatial source coherence on the radiation of jet noise," *Journal of Sound and Vibration* **55**, 377-394 (1977).

[8] U. Michel, "The role of source interference in jet noise," AIAA Paper 2009-3377, 2009.

[9] R. Reba, S. Narayanan, and T. Colonius, "Wave-packet models for large-scale mixing noise," *International Journal of Aeroacoustics* **9**, 533-558 (2010).

[10] B. M. Harker, K. L. Gee, T. B. Neilsen, A. T. Wall, and M. M. James, "Phased-array measurements of full-scale military jet noise," AIAA Paper 2014-3069, 2014.

[11] B. L. Clarkson, "Correlation of pressures around a jet engine," Proceedings of WADC University of Minnesota Conference on Acoustical Fatigue, WADC TR 59-676 (Mar. 1961), pp. 85-98.

[12] H. V. Fuchs, "Space correlations of the fluctuating pressure in subsonic turbulent jets," *Journal of Sound and Vibration* **23**, 77-99 (1972).

[13] H. V. Fuchs, "Application of acoustic mirror, telescope and polar correlation techniques to jet noise source location," *Journal of Sound and Vibration* **58**, 117-126 (1978).

[14] M. J. Fisher, M. Harper-Bourne, and S. A. L. Glegg, "Jet engine noise source location: The polar correlation technique," *Journal of Sound and Vibration* **51**, 23-54 (1977).

[15] C. K. W. Tam, "Influence of nozzle geometry on the noise of high-speed jets," *AIAA Journal* **36**, 1396-1400 (1998).

[16] C. K. W. Tam, M. Golebiowski, and J. M. Seiner, "On the two components of turbulent mixing noise from supersonic jets," AIAA Paper 96-1716, 1996.

[17] S. A. Kumar, N. Karthikeyan, and L. Venkatakrishnan, "Correlation Studies in the Acoustic Far-Field of Non-ideally Expanded Supersonic Jets," AIAA Paper 2013-2082, 2013.

[18] J. Liu, A. T. Corrigan, K. Kailasanath, N. S. Heeb, and E. J. Gutmark, "Numerical Study of Noise Sources Characteristics in An Underexpanded Jet Flow," AIAA Paper 2014-2604, 2014.

[19] J. Panda and R. G. Seasholtz, "Experimental investigation of density fluctuations in high-speed jets and correlation with generated noise," *Journal of Fluid Mechanics* **450**, 97-130 (2002).

[20] J. Panda, R. G. Seasholtz, and K. A. Elam, "Investigation of noise sources in high-speed jets via correlation measurements," *Journal of Fluid Mechanics* **537**, 349-385 (2005).

[21] D. Papamoschou, P. J. Morris, and D. K. McLaughlin, "Beamformed flow-acoustic correlations in high-speed jets," AIAA Paper 2009-3212, 2009.

[22] W. J. Baars, C. E. Tinney, N. E. Murray, B. J. Jansen, and P. Panickar, "The effect of heat on turbulent mixing noise in supersonic jets," AIAA Paper 2011-1029, 2011.

[23] T. F. Brooks and W. M. Humphreys Jr, "Extension of DAMAS phased array processing for spatial coherence determination (DAMAS-C)," AIAA Paper 2006-2654, 2006.

[24] T. F. Brooks and W. M. Humphreys, "A deconvolution approach for the mapping of acoustic sources (DAMAS) determined from phased microphone arrays," *Journal of Sound and Vibration* **294**, 856-879 (2006).

[25] J. S. Bendat and A. G. Piersol, *Random Data: Analysis and Measurement Procedures*, 4th ed. (John Wiley & Sons, Hoboken, NJ, 2010), pp. 109-503

[26] S. R. Venkatesh, D. R. Polak, and S. Narayanan, "Beamforming algorithm for distributed source localization and its application to jet noise," *AIAA Journal* **41**, 1238-1246 (2003).

[27] S. S. Lee and J. Bridges, "Phased-Array Study of Dual-Flow Jet Noise: Effect of Nozzles and Mixers," AIAA Paper 2006-2647, 2006.

[28] R. Schlinker, S. Liljenberg, D. Polak, K. Post, C. Chipman, and A. Stern, "Supersonic Jet Noise Source Characteristics & Propagation: Engine and Model Scale," AIAA Paper 2007-3623, 2007.

[29] T. Suzuki and T. Colonius, "Instability waves in a subsonic round jet detected using a near-field phased microphone array," *Journal of Fluid Mechanics* **565**, 197-226 (2006).

26

[30]A. T. Wall, K. L. Gee, M. M. James, K. A. Bradley, S. A. McInerny, and T. B. Neilsen, "Near-field noise measurements of a high-performance military jet aircraft," *Noise Control Engineering Journal* **60**, 421-434 (2012).

[31]T. B. Neilsen, K. L. Gee, A. T. Wall, and M. M. James, "Similarity spectra analysis of high-performance jet aircraft noise," *Journal of the Acoustical Society of America* **133**, 2116-2125 (2013).

[32]T. B. Neilsen, K. L. Gee, and M. M. James, "Spectral Characterization in the Near and Mid-field of Military Jet Aircraft Noise," AIAA Paper 2013-2191, 2013.

[33]T. B. Neilsen, K. L. Gee, A. T. Wall, M. M. James, and A. A. Atchley, "Comparison of supersonic full-scale and laboratory-scale jet data and the similarity spectra for turbulent mixing noise," *Proceedings of Meetings on Acoustics* **19**, 040071 (2013).

[34]K. L. Gee, V. W. Sparrow, M. M. James, J. M. Downing, C. M. Hobbs, T. B. Gabrielson, and A. A. Atchley, "The role of nonlinear effects in the propagation of noise from high-power jet aircraft," *Journal of the Acoustical Society of America* **123**, 4082-4093 (2008).

[35]P. Jordan and T. Colonius, "Wave packets and turbulent jet noise," *Annual Review of Fluid Mechanics* **45**, 173-195 (2013).

[36]M. Kearney-Fischer, "A model function for jet noise events at aft angles and what it says about the statistical relationships of the events," *Journal of Sound and Vibration* **338**, 217-236 (2015).

[37]C. K. Tam and S. Parrish, "Noise of high-performance aircrafts at afterburner," AIAA Paper 2014-2754, 2014.

[38]A. T. Wall, K. L. Gee, T. B. Neilsen, B. M. Harker, S. A. McInerny, R. C. McKinley, and M. M. James, "Investigation of multi-lobed fighter jet noise sources using acoustical holography and partial field decomposition methods," AIAA Paper 2015-XXXX, 2015.

[39]T. A. Stout, K. L. Gee, T. B. Neilsen, A. T. Wall, and M. M. James, "Intensity analysis of peak-frequency region in noise produced by a military jet aircraft," *Proceedings of Meetings on Acoustics* **20**, 040010 (2014).

[40]A. T. Wall, K. L. Gee, T. B. Neilsen, R. L. McKinley, and M. M. James, "Military jet noise source imaging using multisource statistically optimized near-field acoustical holography," *Journal of the Acoustical Society of America* (Submitted 2015).

[41]K. Viswanathan, "Mechanisms of jet noise generation: classical theories and recent developments," *International Journal of Aeroacoustics* **8**, 355-407 (2009).

American Institute of Aeronautics and Astronautics